Detached Eddy Simulation of Partially Premixed Unstable Flames

By

Shadab Ejaz

(Registration No: 00000330213)

Department of Computational Engineering

School of Interdisciplinary Engineering and Sciences

National University of Sciences & Technology (NUST)

Islamabad, Pakistan

October 2024

Detached Eddy Simulation of Partially Premixed Unstable Flames

By

Shadab Ejaz

(Registration No: 00000330213)

A thesis submitted to the National University of Sciences and Technology, Islamabad,

in partial fulfillment of the requirements for the degree of

Master of Science in

Computational Science and Engineering

Supervisor: Dr. Absaar Ul Jabbar

School of Interdisciplinary Engineering and Sciences

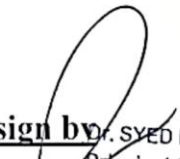National University of Sciences & Technology (NUST)

Islamabad, Pakistan

October 2024

THESIS ACCEPTANCE CERTIFICATE

Certified that final copy of MS/MPhil thesis written by **Mr Shadab Ejaz** Registration No. **330213** of __SINES__ has been vetted by undersigned, found complete in all aspects as per NUST Statutes/Regulations, is free of plagiarism, errors, and mistakes and is accepted as partial fulfillment for award of MS/MPhil degree. It is further certified that necessary amendments as pointed out by GEC members of the scholar have also been incorporated in the said thesis.

Signature with stamp: _____

Assistant Professor
SINES - NUST, Sector H-12
Islamabad

Name of Supervisor: Dr Ahsaan Ul Jabbar

Date: 10 Oct 2024

Signature of HoD with stamp: _____

Dr Fouzia Malik
HoD Sciences
Professor
SINES - NUST Sector H-12
Islamabad

Date: 10-10-2024

Countersign by Dr. SYED IRTIZA ALI SHAH
Principal & Dean
Signature (Dean/Principal): _____ SINES - NUST, Sector H-12
Islamabad.

Date: _____

AUTHOR'S DECLARATION

I Shadab Ejaz hereby state that my MS thesis titled "Detached Eddy Simulation of Partially Premixed Unstable Flames" is my own work and has not been submitted previously by me for taking any degree from National University of Sciences and Technology, Islamabad or anywhere else in the country/ world.

At any time if my statement is found to be incorrect even after I graduate, the university has the right to withdraw my MS degree.

Name of Student: Shadab Ejaz
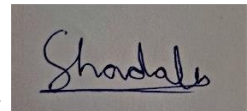
Date: 10th October 2024

PLAGIARISM UNDERTAKING

I solemnly declare that research work presented in the thesis titled "Detached Eddy Simulation of Partially Premixed Unstable Flames" is solely my research work with no significant contribution from any other person. Small contribution/ help wherever taken has been duly acknowledged and that complete thesis has been written by me.

I understand the zero-tolerance policy of the HEC and National University of Sciences and Technology (NUST), Islamabad towards plagiarism. Therefore, I as an author of the above titled thesis declare that no portion of my thesis has been plagiarized and any material used as reference is properly referred/cited.

I undertake that if I am found guilty of any formal plagiarism in the above titled thesis even after award of MS degree, the University reserves the rights to withdraw/revoke my MS degree and that HEC and NUST, Islamabad has the right to publish my name on the HEC/University website on which names of students are placed who submitted plagiarized thesis.

Student Signature:

Name: Shadab Ejaz

DEDICATION

This work is dedicated to my family, who has always been a source of unwavering

support and constant motivation for me in all my endeavours

ACKNOWLEDGEMENTS

TABLE OF CONTENTS

LIST OF TABLES

LIST OF FIGURES

5

LIST OF SYMBOLS, ABBREVIATIONS AND ACRONYMS

Abbreviation	Full Term
CFD	Computational Fluid Dynamics
PDF	Probability Density Function
NOx	Oxides of Nitrogen
DLR	German Aerospace Center
DES	Detached Eddy Simulations
FPV	Flamelet/Progress Variable
EDC	Eddy Dissipation Concept
SAS	Scale Adaptive Simulation
DNS	Direct Numerical Simulation
RANS	Reynolds Averaged Navier-Stokes
URANS	Unsteady Reynolds Averaged Navier-Stokes
LES	Large Eddy Simulations
EDM-FRC	Eddy Dissipation Model-Finite Rate Chemistry
FGM	Flamelet Generated Manifold
CMC	Conditional Moment Closure
TFM	Thickened Flame Model

ORZ	Outer Recirculation Zone
IRZ	Inner Recirculation Zone
SST	Shear Stress Transport
SGS	Subgrid Scale
RSM	Reynolds Stress Model
RMS	Root-Mean-Square
PSR	Perfectly stirred reactor
PFR	Plug flow reactor

List of Symbols

ρ	Density
y_i	Mass fraction of species i
$\boldsymbol{u}$	Velocity vector
t	time
$\boldsymbol{V}_i$	Mass diffusion velocity of species i
w_i	Chemical production rate of species i
N_s	Number of chemical species
p	Normal stress
τ	Viscous stress tensor
f_i	body force per unit mass of the species i
μ	Molecular viscosity
$\mathbf{S}$	Strain rate tensor
μ_B	Bulk viscosity
$\mathbf{I}$	Identity Tensor
e	Mixture internal energy per unit mass
k	Kinetic energy per unit mass
$\boldsymbol{q}$	Heat flux vector

κ	Thermal conductivity
T	Temperature
h_i	Enthalpy per unit mass of the species i
$\hat{R}$	Universal gas constant
$D_{T,i}$	Thermal mass diffusion coefficient of species i
D_{ij}	Binary mass diffusion coefficient matrix
x_j	Mole fraction of species j
$\boldsymbol{q_R}$	Radiative Heat Flux vector
M_i	molecular mass of species i
$\overline{U}$	Mean velocity
u'	Transient velocity fluctuations
G	LES filter function
Δ	LES filter cutoff width
τ_{ij}	SGS stress tensor
$\overline{S_{ij}}$	LES resolved scale strain rate
C_s	Smagorinsky constant
ω	Specific dissipation rate
β^*	DES model constant for LES-like behaviour formulation

Da	Damkohler Number
τ_χ	Diffusive time scale
τ_c	Chemical time scale
u_L/s_L	Laminar flame speed
c	Reaction progress variable
Le	Lewis number
δ_L	Laminar flame thickness
u_T	Turbulent flame thickness
χ_{st}	Scalar dissipation rate
Z	Mixture fraction
ℓ	Turbulent length scale
ℓ_F	Flame thickness
$u_{T,p}$	Mean partially-premixed turbulent velocity
$\tilde{P}$	Filtered probability
ζ	EDC length fraction of fine structures
τ^*	EDC time scale for mass exchange
c_ζ	EDC volume constant
ν	Kinematic viscosity

ϵ	Turbulent dissipation rate
$\overline{R_\iota}$	Reaction rate of fine structures in EDC
Y_i^*	Fine structure mass fraction of species i
χ	Reacting fraction of fine structures (EDC)
Y_i°	Bulk fluid mass fraction of ith species (EDC)
φ	Species mass fraction vector (FPV)
ω	Chemical source term (FPV)
α_t	Turbulent diffusivity (FPV)
α_z	Mixture fraction diffusivity (FPV)
α_C	Progress variable diffusivity (FPV)
$\emptyset(Z, C)$	Scalar as a function of Z and C (FPV)
$\tilde{P}(Z, C)$	Joint subgrid probability density function (FPV)
Ψ_0	Flamelet library parametric variable (FPV)
R_F	Fuel reaction rate (EDM)
$\bar{c}_f$	Mean fuel concentration (EDM)
ε	Turbulent kinetic energy scalar dissipation rate (EDM)
r_f	Stoichiometric mass flow rate of oxygen (EDM)
$[I]$	Concentration of species I

A	Reactant limiting constant (EDM)
B	Product limiting constant (EDM)
W_I	Molecular weight of the species I (EDM)
F_S	Forward reaction rate (EDM-FRC)
B_S	Backward reaction rate (EDM-FRC)
m	Mass flow rate
Q_i	LES-CMC conditioning filter
η	Local mixture fraction space (LES-CMC)
ψ_η	Fine-grained PDF (LES-CMC)
$\widetilde{W}$	Filtered chemical source term (LES-CMC)
$\widetilde{q_{R_\eta}}$	Conditionally filtered radiation term (LES-CMC)
T_a	Activation temperature (LES-TFM)
Σ	SGS flame surface density (LES-TFM)
Ξ	SGS flame wrinkling factor (LES-TFM)

ABSTRACT

Fuel-lean combustion is an area of significant interest in the domain of numerical combustion modelling as it results in the lowering of the emissions of pollutants like CO and NO_x from the combustion chamber. However, the application of fuel-lean combustion also leads to flame blowout, which is why flame stabilization mechanisms like the imparting of swirling motion to the reactants are important to bring the instabilities resulting from lean combustion under control. This work presents the numerical simulation of a benchmark experimental analysis of lean combustion in a dual swirl partially premixed combustor using the Flamelet/Progress Variable (FPV) and Eddy Dissipation Concept (EDC) combustion modelling techniques along with the Detached Eddy Simulations turbulence modelling approach. Performance of each model is analyzed based on its accuracy in capturing time-averaged parameters like axial, radial and swirl velocities, temperatures, mixture fractions and species mass fractions, along with important flow features like the development of recirculation zones. The numerical simulations were set up and executed in the ANSYS Fluent CFD solver, and the reaction kinetics for the Eddy Dissipation Concept were modelled using the GRI Mech 2.11 chemical kinetic mechanism. The FPV approach achieved a considerably higher level of accuracy in capturing the thermochemical parameters compared to EDC, which significantly overpredicted the fuel consumption rate and time-averaged temperatures, while also predicting an unconventional inner recirculation zone profile. Following the validation analysis, a parametric analysis was performed using three combustor configurations featuring distinct inner swirler angles of 60, 62, and 64 degrees respectively. The major differences between the predicted flow features of the three geometries included a broadened inner recirculation zone for the 62 degrees configuration and a considerably narrow inner recirculation zone for the 64 degrees configuration, which also predicted a highly pronounced outer recirculation zone where mixing and reactions dominated as opposed to the inner recirculation zone.

Keywords: partially premixed combustion, recirculation zone, detached eddy simulations, flamelet progress variable, eddy dissipation concept, Mixture fraction

Chapter 1: Introduction

Gas turbine combustors have the utmost importance in the aviation industry, as they are used to power the aero engines for thrust generation. Increasing air traffic over the years has continued to raise environmental concerns, as the gas turbine emissions contain harmful combustion byproducts like CO and NOx that contribute to the climate crisis [1], due to which various regulations have been passed over the years by the International Civil Aviation Organization (ICAO) committee on Aviation Environmental Protection (CAEP) to limit the emission of pollutant gases [2]. To keep in line with the ever-updating regulations limiting the harmful aero emissions, gas turbine combustion technology has also experienced continuous upgrades and modifications over the years. One such approach is lean combustion, which is characterized by the reduction of fuel from the prescribed stoichiometric ratio for hydrocarbon burning [3]. While lean combustion reduces the concentration of NOx and CO in the emissions, it also leads to instabilities in the combustion process like blowoff [4][5] and thermoacoustic oscillations [6][7], which are caused by inefficient mixing due to deviation from stoichiometric ratio. One of the methods to overcome the problem of inefficient mixing in lean combustion is the introduction of components that ensure quick, efficient mixing, like swirlers, which impart angular momentum to the incoming stream of air, leading to rapid mixing between the reactants upon entering the chamber.

Stabilization of lean flames approaching the blowoff limit is a topic of special interest in the field of computational fluid dynamics because of the reduction in pollutant emissions associated with it in practical applications. Various Numerical studies over the years have investigated lean combustion for various applications, and testing of various numerical models to replicate lean combustion in different configurations is important in developing an acceptable trade-off between computational efficiency and accuracy. An important benchmark study in this context is the analysis of dual swirl, partially premixed combustion in a gas turbine combustor by DLR [8][9] which has spurned various numerical validation studies testing the accuracy of different turbulence and combustion modelling techniques respectively.

This thesis aims to perform a numerical validation analysis of the experimental investigation of lean partially premixed flames by DLR using the turbulence-chemistry modelling framework provided in *ANSYS Fluent*, which will be done on a 3D computational domain consisting of the experimental setup.

1.1 Numerical Combustion Modelling

In computational fluid dynamics, combustion modelling is considered one of the most computationally intensive domains. A conventional flow analysis solves the momentum, continuity, and energy equations to resolve, or directly simulate the turbulent flow features, which are guided by the initial and boundary conditions. For the numerical analysis of combustion phenomena, however, an additional layer of complexity is added by the turbulence-chemistry interactions. Besides turbulence modelling, a combustion analysis requires the incorporation of additional equations to solve for species production and consumption resulting from chemical reactions, as well as the determination of flame dynamics [10]. These equations are then coupled with the turbulence model to determine species distribution and the overall flow features.

1.2 Reaction Kinetics in Combustion Modelling

The accuracy of any combustion analysis is significantly dictated by the level of detail with which the reaction kinetics are incorporated. A combustion process realistically consists of several reaction steps consisting of different species, each with distinct reaction rates that are nonlinear functions of physical and chemical parameters. However, the need for reduction of the computational cost of such analyses requires a simplification of the reaction kinetics. The simplest way to do so is to assume fast (one-step) chemistry, in which the reactants are instantly oxidized without any intermediary reaction steps. While this approach suits relatively simpler numerical setups, more complex setups require a greater level of detail to capture the flow dynamics more accurately. For such cases, there exist reaction kinetic mechanisms that are significantly reduced from the detailed mechanisms but incorporate a greater level of detail compared to fast chemistry [11].

1.3 Fuel-lean Combustion

Fuel-lean, or simply lean combustion, has garnered a great deal of research interest in numerical and experimental combustion studies over the years. The main principle behind lean combustion is the reduction of the mass flow rate of fuel from the prescribed stoichiometric value (the flow rate of the fuel required for the reactants to be completely consumed in a chemical reaction). While the reduction of the fuel flow rate from the stoichiometric value can lead to unstable combustion, a major benefit of this approach is the reduction of the production of pollutants like oxides of nitrogen (NOx) [12]. For this reason, combustion applications in

various industries rely on fuel-lean combustion to keep in line with the environmental regulations to ensure minimum emissions of pollutants.

1.4 Combustion Regimes

An important aspect of numerical combustion modelling is the classification of the combustion regime most suited to the computational setup. The three major categories of combustion regimes are non-premixed, premixed, and partially premixed respectively. While numerical modelling approaches distinguishing each regime will be covered in the next chapter, their basic differences can be best explained in terms of the combustor configurations associated with each regime. Non-premixed combustion is characterized by the introduction of reactants directly into the chamber from separate streams and allowing them to achieve stoichiometric mixing within the chamber through diffusion, as shown in figure 1.1. As non-premixed combustion relies on diffusive mixing, the resulting flames are referred to as diffusion flames. Combustor configurations associated with the premixed regime have a separate compartment ahead of the chamber called plenum, in which the reactants are allowed to perfectly mix before being introduced to the chamber, as seen in figure 1.1. Partially premixed combustion, as the name suggests, is a trade-off between the other two regimes. The configuration of a partially premixed combustor resembles that of a non-premixed one, but an additional component placed ahead of the chamber imparts angular momentum to the incoming reactants, causing them to mix rapidly upon entering the chamber, which results in a mixing process that is guided evenly by diffusion and turbulence.
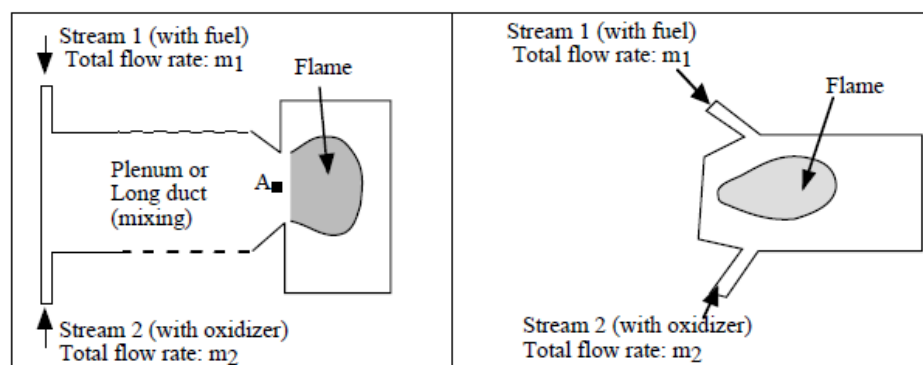
Figure 1.1: Configurations associated with premixed (left) and non-premixed (right) regimes respectively [10]

1.5 Problem Statement

Despite the advancement in computational capabilities to simulate turbulent combustion, high fidelity modelling approaches for combustion analysis are still considered computationally expensive, and there is still room for application of numerical models for validating the benchmark experimental case mentioned above which achieves a compromise in the computational cost without degrading the replication of the experimental results to a great degree. One such modelling technique is the *Detached Eddy Simulations (DES)* turbulence model, and it remains to be investigated whether it achieves an acceptable tradeoff between computational cost and accuracy in replicating the results of partially premixed unstable flames that are near the extinction limit.

Another relatively unexplored area in combustion modelling is the investigation of flow features as the result of varying combustor geometry, which could be important in observing the level at which certain physical and numerical factors influence the prediction of turbulence-chemistry interactions.

1.6 Thesis Objectives

The numerical studies conducted over the years validating the DLR experimental analysis have utilized various turbulence models, combustion models, and chemical kinetic mechanisms. As per the author's knowledge, no such validation analysis has been conducted using the *Detached Eddy Simulations* (DES) turbulence model, and no parametric study involving the lean combustion analysis conducted in this experimental study has been found in the public domain either. Based on this research gap, the main objectives of this study are as follows:

- Numerical validation analysis of the fuel-lean combustion case of the DLR dual swirl experimental study using the *Detached Eddy Simulations (DES)* turbulence model.
- A comparative analysis between the predictions of two different combustion models and chemical kinetic mechanism combinations, namely 1) Eddy Dissipation Concept and GRI-Mech 2.11, and 2) Flamelet/Progress Variable approach and joint PDF approach.
- A parametric analysis involving the variation of the inner swirler angles of the combustor geometry to observe the changes in flow features and turbulence-chemistry interactions resulting from increasing swirler angles.

- A comparison between the results of this study and similar numerical studies undertaken in the past to determine the accuracy of the numerical setup utilized.

1.7 Methodology

The study was initiated by a literature review of the benchmark experimental study followed by a review of the numerical modelling techniques and studies focused on turbulent combustion, through which the research gap was determined. This was followed by the numerical setup of the domain and a preliminary simulation of non-reactive flow. Based on the observations of the non-reactive analysis, the combustion model was applied, and the unsteady reactive flow was simulated. The final step was post processing, in which results were obtained.

1.8 Thesis Outline

The outline of this thesis is as follows. Chapter 2 overviews the fundamental concepts and modelling techniques used for turbulent combustion modelling, chapter 3 presents a literature review of the benchmark experimental study and relevant numerical case studies, chapter 4 presents the methodology adopted in determining the novelty of research and the numerical setup, chapter 5 discusses the simulation results, while chapter 6 presents the conclusions derived from this analysis.

Chapter 2: NUMERICAL MODELLING OF TURBULENT COMBUSTION

Compared to non-reactive flow, numerical modelling of combustion is relatively more complex and more computationally intensive. This is because the governing equations to solve for turbulent reactive flow not only have to model the turbulent conditions, but also must take the turbulence-chemistry interactions into account.

The three major factors dictating numerical setup, and subsequently the requirement of computational resources for a combustion-related problem are 1) Turbulence model, 2) Combustion model, and 3) Chemical Kinetic Mechanism. The basic governing equations for gaseous combustion of ideal gases, which are valid for thermodynamic equilibrium and chemical nonequilibrium are given as follows [13],

Species:

$$\frac{\partial \rho y_i}{\partial t} + \nabla.(\rho \boldsymbol{u} y_i) = -\nabla.(\rho \boldsymbol{V}_i y_i) + \rho w_i, \quad i = 1, \dots, N_s \tag{2.1}$$

Where ρ represents the species density, y_i represents species mass fraction, $\boldsymbol{u}$ is the velocity vector, $\boldsymbol{V}_i$ is the mass diffusion velocity of species i, and w_i is the chemical production rate of species i, and N_s denotes the number of chemical species

Mass:

$$\frac{\partial \rho \boldsymbol{u}}{\partial t} + \nabla.(\rho \boldsymbol{u}) = 0 \tag{2.2}$$

Momentum:

$$\frac{\partial \rho \boldsymbol{u}}{\partial t} + \nabla.(\rho \boldsymbol{u} \boldsymbol{u}) = -\nabla p + \nabla.\tau + \rho \sum_i y_i f_i \tag{2.3}$$

Where the normal stress is denoted by p, τ is the viscous stress tensor, and f_i is the body force per unit mass of the species i.

Viscous stress:

$$\tau = 2\mu \left[\mathbf{S} - \frac{1}{3}(\nabla.\boldsymbol{u})\mathbf{I} \right] + \mu_B (\nabla.\boldsymbol{u})\mathbf{I} \tag{2.4}$$

where μ is the molecular viscosity, $\mathbf{S}$ is the strain-rate tensor $S_{ij} = \frac{1}{2}(u_{i,j} + u_{j,i})$, μ_B is the bulk viscosity, and $\mathbf{I}$ is the identity tensor.

Energy:

$$\frac{\partial \rho(e + k)}{\partial t} + \nabla.[\rho \boldsymbol{u}(e + k)] = -\nabla.(p\boldsymbol{u}) + \nabla.(\tau.\mathbf{u}) - \nabla.\boldsymbol{q} + \rho \sum_i y_i f_i.(\boldsymbol{u} + \boldsymbol{V_i}) \tag{2.5}$$

Where $e = 2.71828$ is the mixture internal energy per unit mass, k is the kinetic energy per unit mass, and $\boldsymbol{q}$ is the heat flux vector with the following equation,

$$\boldsymbol{q} = -\kappa \nabla T + \sum_i \rho \boldsymbol{V_i} y_i h_i + \hat{R}T \sum_i \sum_j \frac{x_j D_{T,i}}{M_i D_{ij}}(\boldsymbol{V_i} - \boldsymbol{V_j}) + \boldsymbol{q_R} \tag{2.6}$$

Where the first term on the right hand side represents the conduction equation, in which and κ is the thermal conductivity, and T is the temperature. The second term on the right hand side represents the mass diffusion, where h_i is the enthalpy per unit mass of the species i. The third term represents the Dufour effect, which is defined as the heat flux caused by concentration gradients. In the third term, $\hat{R}$ is the universal gas constant, $D_{T,i}$ is the thermal mass diffusion coefficient of species i, D_{ij} is the binary mass diffusion coefficient matrix, and x_j is the mole fraction of species j. The term $\boldsymbol{q_R}$ represents the radiative heat flux vector.

Mass Diffusion:

$$\nabla x_i = \sum_j \frac{x_i x_j}{D_{ij}}(\boldsymbol{V_j} - \boldsymbol{V_i}) + (y_i - x_i)\frac{\nabla p}{p} + \frac{\rho}{p}\sum_j y_i y_j (f_i - f_j) + \sum_j \frac{x_i x_j}{\rho D_{ij}}\left(\frac{D_{T,j}}{y_j} - \frac{D_{T,i}}{y_i}\right)\frac{\nabla T}{T} \tag{2.7}$$

Where the first term on the right-hand side is the Stefan-Maxwell expression, which describes the diffusion velocity of species in a multicomponent system. The second term is the pressure gradient, the third term describes body force, while the fourth term accounts for the Soret effect, which models the thermal diffusion in the system.

The thermodynamic state of each species is defined by the ideal gas equation:

$$p = \rho \sum_i \frac{y_i}{M_i} \widehat{R T} \tag{2.8}$$

Where M_i is the molecular mass of species i.

2.1 Turbulence Modelling

Turbulent non-reactive flows are modelled using governing equations for mass and momentum (Navier-Stokes equations), while reactive flows are modelled using additional governing equations that account for species transport and changes in enthalpy occurring due to chemical reactions in the domain. Turbulent flow modelling aims to either resolve or model the turbulence at the Kolmogorov length scale, at which the turbulent energy of the eddies is dissipated to heat [14].

The solution to highly turbulent flows without applying modelling techniques requires the flow to be resolved up to the smallest turbulent scales. This approach is called the direct numerical solution (DNS) and it requires the Navier-Stokes equations to be solved directly without any subgrid averaging. The application of DNS requires the grid size to be smaller than the Kolmogorov scale in order to capture the flow features properly, due to which the mesh requirement for DNS is extreme. Due to this requirement, DNS is not a practical approach for complex flows considering the computational cost associated with it, due to which turbulence modelling techniques are widely used in academic research based on the computational capabilities at hand. The following subsections cover the major techniques associated with turbulent combustion modelling.

2.1.1 Reynolds Averaged Navier Stokes (RANS)

RANS performs a time-averaging of flow features at all turbulent scales. It operates by distributing every parameter being solved for in the governing equations into two parts: the time-averaged value, and the turbulent fluctuation from the time-averaged value. An example following this approach would be the velocity being described as the sum of the mean value $\bar{U}(x,t)$ and the fluctuating value $u'(x,t)$ for arbitrary values of space and time [15].

$$\boldsymbol{u} = \bar{U}(x,t) + u'(x,t) \tag{2.9}$$

With the mean and fluctuating values separated in the governing equations, the Continuity equation would be as follows,

$$\frac{\partial \boldsymbol{u}_x}{\partial x} + \frac{\partial \boldsymbol{u}_y}{\partial y} + \frac{\partial \boldsymbol{u}_z}{\partial z} = \frac{\partial(\bar{U}_x + u'_x)}{\partial x} + \frac{\partial(\bar{U}_y + u'_y)}{\partial y} + \frac{\partial(\bar{U}_z + u'_z)}{\partial z} =$$
$$\frac{\partial \bar{U}_x}{\partial x} + \frac{\partial \bar{U}_y}{\partial y} + \frac{\partial \bar{U}_z}{\partial z} + \frac{\partial u_x{}'}{\partial x} + \frac{\partial u_y{}'}{\partial y} + \frac{\partial u_z{}'}{\partial z} \qquad (2.10)$$

Since $|u'| \ll |\bar{U}|$, the fluctuation terms are canceled out, leaving only mean values in the continuity equation. The same approach applied to momentum equations, however, introduces new terms in the system representing the influence of turbulent fluctuations, which cannot be neglected. These terms are referred to as the Reynolds stresses, which are modelled through the application of turbulence models. There exist 3 major modelling techniques to solve for the Reynolds stresses, 2 of which are referred to as the linear and nonlinear eddy viscosity models respectively. These models establish a relationship between Reynolds stresses and velocity gradients, mapping them on a parameter called eddy viscosity, which is then calculated. The eddy viscosity models are categorized based on the number of differential equations employed. For example, Spalart-Almaras model has one ODE/PDE, while the more commonly used RANS models k-ε and k-ω solve two ODEs/PDEs.

The eddy viscosity models are computationally friendly, but don't achieve a high level of accuracy for complex configurations. Another RANS-based model called the Reynolds stress model (RSM) overcomes the limitations of the eddy viscosity models by directly modelling the stresses through transport equations. RSM is referred to as second order model, as it models the Reynolds stresses by calculating diffusion and turbulent energy dissipation.

2.1.2 Large Eddy Simulations

Large eddy simulations (LES) is a turbulence modelling approach suited for high fidelity CFD computations. LES operates by resolving the larger turbulent eddies while modelling the subgrid turbulence. Based on this approach, LES requires a higher grid resolution compared to RANS, due to which it has a greater computational requirement. LES also captures turbulent features of the flow to a great extent, only requiring the smallest turbulent scales to be modelled through a subgrid scale (SGS) model, which is an upgrade to the entirely time-averaged flow dynamics of RANS.

To segregate the large eddies to be resolved from the subgrid eddies that need to be modelled, LES applies spatial filtering operation to the instantaneous Navier-Stokes equations [16]. The spatial filtering is defined by a filter function $G(x, x', \Delta)$ as follows,

$$\bar{\emptyset}(x,t) \equiv \int\limits_{-\infty}^{\infty} \int\limits_{-\infty}^{\infty} \int\limits_{-\infty}^{\infty} G(x,x',\Delta)\emptyset(x',t)dx_1' dx_2' dx_3' \tag{2.11}$$

Where $\emptyset(x',t)$ is the original function, $\bar{\emptyset}(x,t)$ is the filtered function, and Δ is the filter cutoff width. The three most commonly utilized filter functions are box, gaussian, and spectral cutoff filters respectively [14].

The LES filtering introduces an unknown SGS stress tensor τ_{ij} in the Navier-Stokes equations, which represents the effects of the SGS motions on the resolved flow and needs to be modelled. There exist various approaches to model the SGS influences on the resolved flow, and most of these SGS models apply the eddy viscosity assumption [17] [18] (Bousinesq's hypothesis) to model the SGS stress tensor with the following formulation,

$$\tau_{ij} = 2\mu_t \overline{S_{ij}} + \frac{1}{3}\delta_{ij}\tau_{ll} \tag{2.12}$$

Where $\overline{S_{ij}}$ is the resolved scale strain rate and μ_t is the SGS eddy viscosity, which is described as follows by the Smagorinsky model,

$$\begin{cases} \mu_t = \rho(C_s\bar{\Delta})^2 S \\ S = \left(2\overline{S_{ij}}\,\overline{S_{ij}}\right)^{\frac{1}{2}} \\ \Delta = (\Delta x \Delta y \Delta z)^{\frac{1}{3}} \end{cases} \tag{2.13}$$

Where C_s is the Smagorinsky constant, which depends on the proximity of the flow to the domain walls and varies from 0.1 to 0.18. A further development on the Smagorinsky model [19] proposed a dynamic value of C_s, which varied depending on local flow conditions.

2.1.3 Detached Eddy Simulations

Detached Eddy Simulations (DES) is a hybrid modelling approach which selectively applies both LES and RANS approaches to model turbulence [20]. DES aims to lower the computational cost associated with LES while improving the level to which turbulent flow dynamics are captured by RANS. The application of the modelling approach typically depends on the proximity of the flow to the walls. A RANS-like model is conventionally applied in the

near-wall region, where computational efficiency is required to resolve the boundary layer, while the LES-like approach is applied for flows that are massively separated from the walls.

In the DES approach, RANS and LES are not explicitly separated, but a single model is applied based on grid spacing and flow characteristics. This model adaptation is achieved through the specification of a modified length scale, called the DES length scale (LDES) [21]. The LDES is defined as the minimum of the RANS length scale (LRANS) and the scale proportional to the local grid spacing (CDESΔ). The ANSYS Fluent solver treats CDESΔ as a "calibration constant" with a value of 0.65 [22].

$$LDES = \min(LRANS, CDES\Delta) \tag{2.14}$$

The grid spacing in the boundary layers is usually larger than the boundary layer thickness, and in those regions LRANS is smaller than CDESΔ, which prompts the RANS-like modelling to be applied, and vice versa. A numerical study of dual swirl partially premixed combustion utilizing the DES model [23] employed the SST-k-ω model for the RANS-like behaviour, based on which the value of LRANS (mentioned in the publication as $L_{t,SST}$) was as follows,

$$LRANS(SST) = \frac{\sqrt{k}}{\beta^* \omega} \tag{2.15}$$

Where k is the turbulent kinetic energy, ω is the specific dissipation rate, and β^* is a model coefficient.

This hybrid approach is confronted by the treatment of the "gray areas" where the transition between the LES-like and RANS-like conditions occurs. This transition depends on the grid and flow characteristics, which is why grid sizing carries great importance for the application of DES, and a sufficient resolution must be applied to facilitate LES-like behaviour for separated flow.

2.2 Numerical Modelling of Combustion Regimes

As mentioned in chapter 1, the three major classifications of combustions based on the type of mixing are non-premixed, premixed, and partially premixed. In this subsection, the major differences in the numerical modelling of each type will be overviewed.

2.2.1 Non-Premixed Combustion

A non-premixed system is characterized by the introduction of fuel and oxidizer from separate inlets, and their mixing is guided mainly by the process of diffusion. Non-premixed configurations are the simplest to design and build since they do not require complex plenum designs for premixing the reactants. The process of non-premixed combustion however, is difficult to control. This is because reactions take place in zones where the reactants have mixed stoichiometrically through diffusion, and consequently the flame lies in those regions as well.

The diffusive nature of non-premixed flames ensures that they do not propagate upstream or downstream. While this enhances the safety of the combustion process, it also means that turbulence greatly influences the flow field, and can lead to the extinction of flames by disturbing the stoichiometric reaction zones. Since the findings on the effects of turbulence in diffusion flames [24], there has been a significant amount of research on this topic, and the development of numerical models for turbulent reactive flows has been largely built on these foundational studies [25] [26] [27].

The two extreme cases in diffusion flames are characterized by the diffusive time and chemical time. Diffusive time (τ_χ), or residence time, is the time taken for the reactants to diffuse and mix stoichiometrically in the reaction zone, while chemical time (τ_c) is characterized by the time taken to reach 1/e of the initial reactant concentration. In the case of diffusion flames, the Damköhler number (Da) couples the two quantities together and defines the extreme cases for turbulent diffusion combustion.

$$Da = \frac{\tau_\chi}{\tau_c} \tag{2.16}$$

For the case of perfect premixing, infinitely fast chemistry is assumed ($\tau_c \rightarrow 0$), and Da $\rightarrow \infty$. For the case of pure mixing without combustion, Da $\rightarrow 0$. For chemistry controlled reactions, Da $\ll$ 1, while for transport controlled reactions that are characteristic of non-premixed combustion, Da $\gg$ 1.

2.2.2 Premixed Combustion

As mentioned in the previous chapter, premixed combustion is characterized by perfect mixing of the reactants prior to entering the chamber. In a typical premixed combustion cycle, heat from the reaction products diffuses upstream towards the incoming reactants and this heat

transfer from the products triggers a reaction [28]. A premixed combustion system is not limited by the mixing rate of individual reactants but is instead governed by the thermal diffusion rate as well as the rate of mixing between reactants and products, and all the controlling parameters in the premixed system are enhanced by increasing turbulence [29].

The simplest instance of a premixed flame is represented by an unstretched laminar flame, which travels to the dormant reactants at a speed called the *laminar flame speed* denoted by u_L [30] or s_L [29]. The laminar flame speed is based on the primary transport equation for the progress variable c which describes the thermochemical state of the unstretched laminar premixed flames. The transport equation for unstretched laminar flames is developed using a set of assumptions, the most important of which is that of unity Lewis number (Le). Lewis number is the ratio between thermal diffusivity and mass diffusivity, and it has been shown that for turbulent flames it can be assumed to be 1 [31].

The transport equation for c is given as:

$$\rho \frac{Dc}{Dt} = \rho \left(\frac{\partial}{\partial t} + \boldsymbol{u}.\nabla \right) c = \nabla.(\rho D \nabla c) + \rho S \qquad (2.17)$$

Where $\boldsymbol{u}$ is the fluid field velocity, and the density ρ, diffusivity D, and reaction rate S are all functions of c respectively. S is dependent on a variable called the reaction time scale, which is denoted by τ_R. The laminar flame speed is inversely proportional to $(D/\tau_R)^{1/2}$. Several experimental methods to determine the laminar flame speed have been proposed [32], while there also has been notable research to determine laminar flame speeds specifically for lean combustion mechanisms [33].

Another important characteristic of laminar flames is the *laminar flame thickness*, denoted by δ_L. Mathematically, several ways have been proposed to describe δ_L [34], and one of the simpler definitions attributes it to the distance between the regions of 5% and 95% temperature rise respectively. Another definition associates δ_L with the thermal diffusivity of reactants D_r and the laminar flame speed u_L as follows,

$$\delta_L \equiv \frac{D_r}{u_L} \qquad (2.18)$$

For cases involving turbulent diffusion of reactant stream, the flame propagates towards the incoming reactants with a much greater velocity, which is referred to as the turbulent flame

speed, denoted as u_T. Both the flame speed and flame thickness of turbulent flames are greater than those of laminar flames. Several methods have been proposed to determine the turbulent flame speed for premixed flames, and a relatively simpler approach describes it as follows,

$$\frac{u_T}{u_L} = 1 + \alpha \left(\frac{u'}{u_L}\right)^n \qquad (2.19)$$

where u' is the turbulent intensity, while α and n are model parameters respectively [28].

Several reviews discuss the formulation of these fundamental concepts for premixed combustion modelling and describe in detail the link between the structure and the thermochemical properties of the flame respectively [35] [36] [37] [38].

2.2.3 Partially Premixed Combustion

The combustion regime for the solution of any combustion-related problem is determined mainly by the combustor geometry, but there exist cases that are considered as tradeoffs between the premixed and non-premixed regimes, and are modelled as partially premixed [39]. The injection mechanism of a partially premixed combustor is built like a non-premixed one but features rapid mixing of the reactants guided by turbulence prior to the establishing of the reaction zone [40]. As a result of this mixing, the flow no longer remains entirely diffusive, and the stoichiometric/reaction zone does not remain the solely important feature in the combustion domain. Furthermore, swirl-stabilized partial-premixing paves way for another phenomenon – the development of recirculation zones, which recirculate hot gases upstream [8], leading to stabilization of flame due to enhanced mixing between fuel, oxidizer, and burnt mixtures. Certain instances of partially premixed systems that feature high ratios of cooled recirculation zones have delivered a simultaneous reduction of No_x and soot emissions respectively for diesel engines [41].

Partially premixed combustion in gas-turbine combustors is characterized by the lift-off and stabilization of flames downstream of the fuel injector channel. It has been observed in earlier studies that flame tends to lift-off from the nozzle base when its exit velocity u_0 exceeds a certain critical value, and will be stabilized at the point where the mean flow velocity and burning velocity match [42]. A reinforcement to the flame-lift off theory [43] argued that a lift-off event becomes likely to occur when the probability of scalar dissipation rate χ_{st}, which governs the diffusion flamelets, falls below a certain threshold. A parametric study [44]

conducted to observe the variation of methane flame lift-off height with different air-fuel ratios, nozzle diameters d, and exit velocities concluded that the normalized lift-off height (H/d) varies linearly with u_0, and that blow-off occurs after the value of H/d exceeds 40.

A typical instance of partial premixing occurring in a combustion setup is characterized by a "triple flame" zone [45], and its structure contains regions between the minimum and maximum mixture fractions ($Z_{min} < Z < Z_{max}$) respectively, including the stoichiometric mixture fraction (Z_{st}) region. A triple flame has three branches: leading edge (called the triple point) that propagates along a surface in the vicinity of the stoichiometric region, a premixed lean-side branch, that lies on the fuel-lean side of the leading-edge propagation surface, and a premixed rich-side branch, which exists on the fuel-rich side of the propagation surface. The flame speed at the triple point is the highest, and it gradually decreases as one moves downstream from the triple point to either of the two branches. For a triple flame with uniform premixed front propagation velocity **u**, the relation for **u** is given as

$$u_L(Z)\sigma(Z) = \boldsymbol{u} \tag{2.20}$$

where u_L and the velocity gradient σ are functions of local mixture fraction Z [46]. The equation mentioned above proposes the same function for the flame propagation speed for each point in the triple flame, based on which a more recent study [47] broke down the propagation speed into laminar and turbulent zones, resulting in the following relation

$$u_T(Z) = u_L(Z) + v'f\{Da(Z)\} \tag{2.21}$$

Where $f\{Da(Z)\} = \Delta s/v'$, and Δs is the difference between the laminar and turbulent flame velocities respectively, while v' is the turbulence intensity. $Da(Z)$ is the conditional Damkohler number which is defined as follows

$$Da(Z) = \frac{u_L(Z)\ell}{v'\ell_F(Z)} = \frac{u_L{}^2(Z)\ell}{v'D} \tag{\#2.22}$$

Where ℓ is the turbulent length scale, ℓ_F is the flame thickness, and D is the diffusivity of the burnt mixture. The mean partially premixed turbulent velocity $u_{T,p}$ is determined as follows

$$(\bar{\rho}u_{T,p}) = \int_0^1 \rho(Z)u_T(Z)\tilde{P}(Z)dZ \tag{2.23}$$

Where $\bar{\rho}$ is the favre-filtered density and $\tilde{P}(Z)$ is the filtered probability of mixture fraction obtained from a presumed PDF function.

The formulations described above were used to numerically simulate the stabilization and lift-off characteristics of a partially premixed turbulent lifted jet flame [48] in a numerical study which utilized the equations for the filtered mixture fraction $\tilde{Z}$, its variance $\widetilde{Z''}$, an equation catering for the location of the premixed flame front denoted by $\tilde{G}$, and an addition equation to solve for the enthalpy $\tilde{h}$. The functions describing the dependence of scalars on mixture fraction Z were calculated using diffusion flamelets, which were classified as either burnt or unburnt. Three different equations were derived to calculate the species mass fractions and enthalpy for the burnt region, the unburnt region, and the flame brush region.

Table 2.1: Characteristics of combustion regimes

Combustion Regime	Reaction mechanism	Distinct mathematical modelling parameter(s)
Non-premixed combustion	Diffusive mixing in the combustion chamber leading to stoichiometric zones	Diffusion time ($\tau\chi$) >> Chemical time (τc)
Premixed combustion	Premixed reactants react with thermally diffused hot products	Laminar flame Speed (u_L) Laminar flame thickness (δ_L) Turbulent flame speed (u_T) Turbulent intensity (u')
Partially premixed combustion	Diffusive mixing aided by a quick turbulent mixing mechanism leading to recirculation zones	Mixture fraction (Z) Flame front location (G) Conditional Damkohler number (Da(Z)) Mean partially premixed turbulent velocity ($u_{T,p}$)

2.3 Combustion Models

The numerical combustion model involves the development of a system of equations and parameters which interact with the governing equations of the turbulence model to provide solution for thermochemical quantities like mixture fraction, species mass fractions, temperature, species concentrations, among others. Combustion models provide a link between the turbulent and chemical changes that the reactive flow goes through to give accurate results for each quantity. This section discusses various combustion models that have been utilized in the analyses of dual-swirl, partially premixed lean combustion in the past, with focus on the two models utilized in this thesis.

2.3.1 Eddy Dissipation Concept

The foundation of Eddy Dissipation Concept (EDC) lies in the assumption that all chemical reactions occur within the fine turbulent structures, called "eddies", and the process of energy transfer occurs from larger to smaller eddies in a process referred to as "energy cascading" [49]. These fine structures have infinitesimal, subgrid scale lengths in 2 dimensions but are considerably larger in the third dimension, due to which they are also referred to as "slabs", "sheets" or "vortex tubes". Based on this approach, the fine structures are considered as perfectly stirred reactors (PSRs). This process culminates in the dissipation of energy from the smallest eddy to heat.

The EDC approach models the transfer of turbulent energy towards the fine structures, and determines the reaction rates occurring in these structures.

The cascading process in characterized by the mass exchange between the reactive fine structures and the surrounding bulk fluid, which is assumed to be a non-reactive zone. This mass exchange during the cascading process is taken as a basis to determine the reaction rates in EDC formulations. As a result, the length fraction of fine structures (ζ) and the time scale for mass exchange between the reaction zones and the surrounding fluid (τ^*) are used in the basic numerical representation of the EDC model.

$$\zeta = c_\zeta \left(\frac{\nu\epsilon}{k^2}\right)^{\frac{1}{4}} \tag{2.24}$$

$$\tau^* = c_\tau \left(\frac{\nu}{\epsilon}\right)^{\frac{1}{2}} \tag{2.25}$$

where c_ζ is a volume constant, c_τ is a time-scale constant, ν is kinematic viscosity, ϵ is turbulent dissipation rate, and k is the turbulent kinetic energy. The reaction rate of the fine structures, $\bar{R}_\iota$, is determined as follows,

$$\bar{R}_\iota = \frac{\bar{\rho}}{\tau^*}\left(\frac{\zeta^2\chi}{1-\zeta^3\chi}\right)(\bar{Y}_i - Y_i^*) \tag{2.26}$$

Where the subscript i denotes chemical species, $\bar{Y}_\iota$ denotes the mean mass fraction of the ith species, and Y_i^* represents the fine structure mass fraction of the species i, and χ is the reacting fraction of fine structures, which is assumed to be unity for highly turbulent structures. After applying assumptions of constant enthalpy and pressure respectively, the system of equations for the PSR is as follows [50],

$$\frac{dY_i}{dt} = \bar{R}_\iota + \frac{1}{\tau^*}\left(Y_i^\circ - Y_i^*\right) \tag{2.27}$$

$$\frac{dh}{dt} = 0 \tag{2.29}$$

$$\frac{dp}{dt} = 0 \tag{2.30}$$

Where Y_i° is the mass fraction of the ith chemical species in the surrounding bulk fluid, and the second term on the right-hand side represents mixing between the fine structures and their surrounding bulk fluid, h is the enthalpy, and p is the pressure. This approach involves dealing with the nonlinearity of the chemical source term, due to which solving this set of equations can become highly computationally intensive. Another issue with this approach is that in some cases it can lead to periodic oscillations of the species mass fraction, making the solution unstable. To overcome these barriers, a proposed simplification [51] takes the mixing term out of consideration, as a result of which only the reaction term remains,

$$\frac{dY_i}{dt} = \bar{R}_\iota \tag{2.31}$$

$$\frac{dh}{dt} = 0 \tag{2.32}$$

$$\frac{dp}{dt} = 0 \tag{2.33}$$

This approach transforms the PSRs to "Plug Flow Reactors" (PFRs), which are assumed to have no back mixing between the fine structures and their surroundings, as opposed to the PSRs, which indicates that while the conditions within PFRs remain adiabatic, there is no mass transfer with the surroundings as in PSRs [52]. Due to this simplification, the PFR approach is considered less accurate compared to the PSR approach, so the choice of approach must be determined taking the complexity of the problem as well as the computational resources into account.

There have been multiple modifications to the numerical definition of the fine structure length scales ζ, leading to minor changes in the reaction rate equation [53][54], and a recent publication proposed dynamic adjustments to the model constants c_ζ and c_τ [55] to cater for slower reaction rates in order to overcome the limitations of the EDC model for Moderate or Intense Low Oxygen Dilution (MILD) combustion.

2.3.2 Flamelet/Progress Variable Approach

The novelty of the flamelet/progress variable (FPV) approach lies in its definition of the structure of a turbulent flame by considering it to be composed of steady one-dimensional diffusion flamelets. The physical and chemical properties of the flamelets are stored in a database called the flamelet library, which consists of pre-computed solutions to flamelet equations.

The precursor to the FPV approach that is widely used today for combustion modelling was the flamelet model proposed by Peters [56]. This initial model was proposed for suitability to non-premixed combustion, and the major assumption behind its mathematical approach was that the reaction rate is guided by the rate of diffusion of the reactants. This assumption is implemented in the model through a coupled diffusion-reaction equation as the species transport equation in the set of governing equations.

$$\frac{\partial \rho y_i}{\partial t} + \nabla.(\rho u y_i) = -\nabla.(\rho V_i y_i) + \rho w_i, \quad i = 1, ..., N_S \qquad (2.34)$$

Where y_i is the mass fraction of species i, u is the velocity magnitude, V_i is the mass diffusion velocity of the ith species, w_i is the chemical production rate of the species i, and N_S is the number of chemical species being considered. A simplification of the species transport

equation and the energy equation, called the steady-flamelet equation, is solved to obtain the relations for the parameters in the flamelet library. The steady-flamelet equation is given as,

$$-\rho \frac{\chi}{2} \frac{\partial^2 \varphi}{\partial Z^2} = \omega \tag{2.35}$$

Where χ is the scalar dissipation rate , Φ is the species mass fraction vector, Z is the mixture fraction, and the chemical source term is represented by ω. The scalar dissipation rate is linked to Z by the following relation,

$$\chi = 2D_z(\nabla Z)^2 \tag{2.36}$$

where the molecular diffusivity of the mixture fraction is represented by *Z*.

The thermochemical parameters of the reactive flow like temperature and species mass fractions are implicitly linked to *Z* and χ, and are obtained using the flamelet library once the steady-flamelet equations solve for these two parameters. The resulting relation between temperature and χ results in an S-shaped curve, the upper branch of which is representative of stable-burning flames while the lower branch depicts the unburnt mixture. The part connecting the two branches represents the unstable regime. An example of such a curve can is shown in **Figure 2.1**.
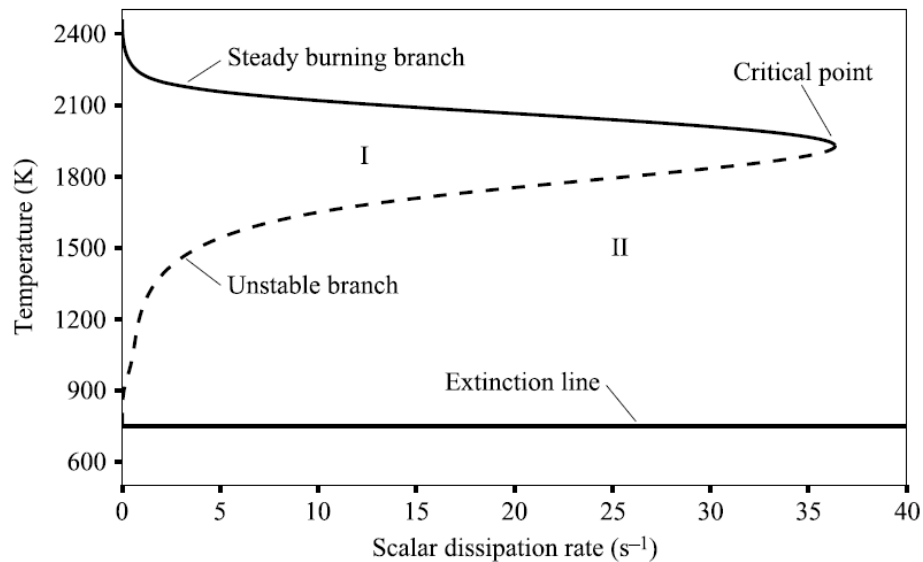

Figure 2.1: The S-shaped curve obtained by solving steady-flamelet equations [57]

A major limitation of the conventional flamelet approach is that it gives inaccurate solutions for flows with lower Damkohler numbers (Da), in which the respective mixing and chemical times become comparable. This phenomenon is observed in flows that undergo repetitive extinction and ignition of flames, which are characteristic of conditions close to the lean blowoff limit. It has also been observed that the dependence of multiple parameters on χ results in multiple solutions for a single value of χ for more numerically advanced cases, due to which the scalar dissipation rate is not a suitable parameter to represent the entire solution space [58].

The FPV approach was proposed to resolve the limitations of the conventional flamelet model by introducing a new variable to map the thermochemical parameters onto, called the *reaction progress variable* (*C*) [57]. There exist other modifications to the flamelet model proposing similar parameters [59][60], but FPV was the first proposition of its kind in which *C* was independent of mixture fraction *Z*. In the FPV formulations, *Z* accounts for all the conserved scalars, while *C* accounts for the chemical reactions occurring in the system. This results in a system represented by two transport equations which provide the complete thermochemical state of the flames. For a system modelled using FPV and LES, the system of equations is,

$$\frac{\partial \bar{\rho} \tilde{Z}}{\partial t} + \nabla . \left(\bar{\rho} \tilde{u} \tilde{Z} \right) = \nabla . [\bar{\rho} (\tilde{\alpha}_z + \alpha_t) \nabla \tilde{Z}] \tag{2.37}$$

$$\frac{\partial \bar{\rho} \tilde{C}}{\partial t} + \nabla . \left(\bar{\rho} \tilde{u} \tilde{C} \right) = \nabla . [\bar{\rho} (\tilde{\alpha}_C + \alpha_t) \nabla \tilde{Z}] + \bar{\rho} \, \tilde{\omega}_c \tag{2.38}$$

Where α_t is the turbulent diffusivity, α_z is the mixture fraction diffusivity, and α_C is the progress variable diffusivity. Variables with the overbar represent the LES-filtered quantities, while tilde signifies density weighted quantities.

When modelled along with LES, the unfiltered (resolved) values of the flow properties are all functions of *Z* and C, and can be obtained through the flamelet library. However, the subgrid variation of mixture fraction *Z* and the progress variable *C*, along with the subgrid values of the conserved scalars (the parameters dependant on *Z* and *C*) are obtained by integrating each scalar over a joint subgrid probability density function (PDF) of *Z* and *C*. The subgrid formulation of a filtered variable ø is as follows,

$$\tilde{\emptyset} = \int \emptyset(Z,C)\,\tilde{P}(Z,C)dZ\,dC \tag{2.39}$$

where $\emptyset(Z,C)$ is obtained through the steady-flamelet library, while the joint subgrid PDF $\tilde{P}(Z,C)$ is the product of the subgrid probability density function of mixture fraction $\tilde{P}(Z)$ and the conditional PDF $\tilde{P}(C|Z)$, which is represented by the following delta function,

$$\tilde{P}(C|Z) = \delta\left(C - \widetilde{C|Z}\right) \tag{2.40}$$

$\widetilde{C|Z}$, the conditional mean, is given by,

$$\widetilde{C|Z} = C(Z,\Psi_0) \tag{2.41}$$

Where ψ is a parametric variable used to determine the steady-state flamelet solutions.

2.3.3 Eddy Dissipation Model

Eddy Dissipation Model (EDM) is actively utilized for simulating non-premixed combustion, as its underlying formulations are developed on the assumption that reactions take place in the domain only after the reactants are perfectly mixed, due to which the chemical time scale is negligible compared to the mixing time [61]. While the model aims to predict the rate of reaction in the domain like the similarly named model Eddy Dissipation Concept (EDC), and both models show dependency on the mixing process, EDC incorporates a greater level of detail mathematically and is suited for more complex systems. While EDC deals with the length scale of fine structures along with the mixing time scale, EDM directly incorporates reactant properties in its basic formulations, and by showing a significant reliance on model constants, includes lesser number of parameters than EDC which is why it is less computationally intensive.

The rate of reaction of fuel R_F for purely diffusive reactions in EDM formulation is given as:

$$R_F = A.\bar{c}_f \left(\frac{\varepsilon}{k}\right) \tag{2.42}$$

where c_f is the time-mean concentration of the fuel, k is the turbulent kinetic energy, and ε is the rate of dissipation of k. A is a model constant which depends on the fuel-oxygen reaction mechanism. This equation is used to solve for regions in the domain where the reaction is

limited by the fuel concentration. For regions where oxygen is the intermittent species, the reaction rate is given as,

$$R_F = A \left(\frac{\bar{c}_{O_2}}{r_f} \right) \left(\frac{\varepsilon}{k} \right) \tag{2.43}$$

where $\bar{c}_{O_2}$ is the time-mean oxygen concentration, while r_f is the amount of oxygen required to completely react with 1kg of fuel.

For premixed or partially premixed flames, the reaction rate equation can be modified to solve for both mixing-dominated and reaction dominated phases. The equation describing reaction rate in the phase dominated by mixing has been described by as follows,

$$R_{S_{EDM}} = A \left(\frac{\varepsilon}{k} \right) \left(\frac{[I]}{v_{sI}{}'} \right) \tag{2.44}$$

Where A is the reactant limiting constant $[I]$ indicates the concentration of species I, and $v_{sI}{}'$ is the exponent of species I for the reactant side.

The corresponding equation for reaction dominated phase is,

$$R_{S_{EDM}} = AB \left(\frac{\varepsilon}{k} \right) \left(\frac{\sum_P [I] W_I}{\sum_P v_{sI}{}''^{W_I}} \right) \tag{2.45}$$

where B is the product limiting constant, $v_{sI}{}''$ is the exponent of species I for the product side, and W_I is the molecular weight of the species I. The equation that gives the lower value of the reaction rate at each instance is chosen as the local reaction rate.

As explained earlier, the EDM formulation relies significantly on the model constants A and B, which is why this model can prove too stringent for complex applications. A recent study proposed a modified EDM approach which dynamically adjusts the value of A based on the local Reynolds Number [62] which led to improved predictions compared to the conventional EDM approach.

A major limitation of EDM is that it is only applicable to cases of infinitely fast chemistry, as its underlying principles, based on which the formulations are derived are suited to reactions with negligible chemical time scales. As per the author's knowledge, all the numerical studies centered on dual swirl partially premixed combustion that have utilized EDM, have overcome

this limitation by combining it with the Finite-Rate Chemistry (FRC) model, which is why more recent studies utilizing this model refer to it as the EDM-FRC model. The FRC model solves for reaction rates in regions where chemical time scale dominates, and is described as follows,

$$R_{S_{FRC}} = F_S \prod_{I=X_1,X_2,\ldots}^{N_S} [I^{v_{sI}'}] - B_S \prod_{I=X_1,X_2,\ldots}^{N_S} [I^{v_{sI}''}] \tag{2.46}$$

where F_s and B_S are the forward and backward reaction rate constants respectively.

2.3.4 Flamelet Generated Manifold

Flamelet Generated Manifold (FGM) approach, proposed initially by van Oijen and de Goey [63] bears similarity to the flamelet approach in terms of considering a flame to be composed of 1D steady laminar flamelets. Like the flamelet approach, FGM stores thermochemical quantities in a flamelet library [64]. However, the difference between the two models is that while the flamelet-based approaches map the thermochemical quantities on only a couple of controlling variables (mixture fraction and progress variable), for FGM, the number of controlling variables can be made to vary depending on the availability of computational resources and the level of complexity of the problem. This allows for greater flexibility in solution. Furthermore, FGM formulations give greater consideration to the processes of diffusion and convection in the colder regions of the flame, due to which the flow features for those regions are predicted with greater accuracy.

In the FGM model, the term "manifold" refers to the number of controlling variables that will be utilized to solve the problem. The simplest instance of FGM (one-dimensional manifold) incorporates only one controlling variable, also called the progress variable (different from the progress variable C in the FPV model) alongside the enthalpy h. The governing equations for enthalpy h and species mass fraction Y_i are used to generate the manifold of 1D steady laminar flamelets. The scalars conserved by the chemical reactions are then used to calculate the burnt mixture properties, while the controlling variable itself is used to determine the properties of the unstable part (between burnt and unburnt regions).

For non-premixed flames, the steady state equation for Y_i is given as follows,

$$m \frac{\partial Y_i}{\partial s} - \frac{\partial}{\partial s}\left(\frac{1}{Le_i}\frac{\lambda}{c_p}\frac{\partial Y_i}{\partial s}\right) = \omega_i^+ - \omega_i^-, \quad i = 1,\dots\dots,N, \tag{2.47}$$

where m is the mass flow rate, s represents the arc length, Le is the Lewis number, λ is the thermal conductivity, c_p is the specific heat, while ω_i^+ and ω_i^- represent the production and reaction parts of the chemical source term respectively. A similar equation is solved for the enthalpy h to obtain the solution of each flamelet in terms of $Y_i(s)$ and $h(s)$.

2.3.5 Conditional Moment Closure

The conditional moment closure (CMC) model was proposed to overcome the limitations of flamelet-based approaches in accurately modelling reactive flows in which the chemical time scale dominates, along with improved predictions for CO and NO mass fractions. There exist two variants of the CMC model to be coupled with the LES [65] and RANS [66] turbulence models. As per the author's knowledge, the only numerical validation study of dual swirl partially premixed combustion that utilized the CMC model coupled it with LES, so the CMC-LES modelling approach will be discussed in this section.

The CMC approach introduces conditional filtering to improve the interaction between the large turbulent eddies and the mixing of species occurring on the small scale. The conditional filter, Q, improves the dependency of the species mass fraction and enthalpy on the local mixture fraction space, which is denoted by η.

$$Q_i = \overline{Y_i|\eta} \equiv \frac{\int_V Y\psi_\eta(\xi(x',t) - \eta)G(x - x',\Delta)dV'}{\bar{P}(\eta)} \tag{2.48}$$

where Y_i is the mass fraction of the i-th species, ξ is the mixture fraction, G is a space filter with filter width Δ, and $\bar{P}(\eta)$ is a filtered PDF (FDF) which is formulated as follows,

$$\bar{P}(\eta) = \int_V \psi_\eta(\xi(x',t) - \eta)G(x - x',\Delta)dV' \tag{2.49}$$

while the ψ_η referred to as "fine-grained PDF", and is given by,

$$\psi_\eta = \delta[\eta - \xi(x,t)] \tag{2.50}$$

where δ represents the dirac-delta function of the expression within the brackets.

The same approach is then followed for deriving a conditional filter for the enthalpy h. The final LES-CMC equations for reactive species transport are,

$$\frac{\partial Q_i}{\partial t} + \widetilde{v}_\eta \nabla Q_i = \widetilde{W}_\eta + \frac{\widetilde{\chi}_\eta}{2}\frac{\partial^2 Q_i}{\partial \eta^2} + e_y \tag{2.51}$$

$$\frac{\partial Q_h}{\partial t} + \widetilde{v}_\eta \nabla Q_h = \widetilde{q_{R_\eta}} + \frac{\widetilde{\chi}_\eta}{2}\frac{\partial^2 Q_h}{\partial \eta^2} + e_h \tag{2.52}$$

where the quantities with tilde represent density-filtered terms, $\widetilde{W}$ is the filtered chemical source term, $\widetilde{\chi}$ is the scalar dissipation rate, $\widetilde{q_{R_\eta}}$ is the conditionally filtered radiation term, while e_y and e_h represent the fluctuations around the respective conditional mean values.

2.3.6 LES-Thickened Flame Model (LES-TFM)

The LES-TFM model aims to enhance the thickness of the flame front in order for it to be resolved by the LES model [67]. A problem often encountered in the flame front modelling is that the flame front thickness δ_l^0 is less than an individual cell size Δ_x, due to which the flame front remains unresolved. The TFM modelling approach aims to artificially increase the flame front thickness while keeping the laminar flame speed s_l^0 the same. The is done by introducing a flame thickening factor F into the laminar flame speed relations.

$$s_l^0 \propto \sqrt{D\overline{W}}, \quad \delta_l^0 \propto \frac{D}{s_l^0} \tag{2.53}$$

where D is the molecular diffusivity and $\overline{W}$ is the mean reaction rate. The above-mentioned relations are altered by multiplying the thickening factor with the diffusivities (F.D) and dividing with the mean reaction rate ($\frac{\overline{W}}{F}$). F is also introduced into the species transport equation for fuel, which then becomes,

$$\frac{\partial \rho Y_F}{\partial t} + \nabla.(\rho \mathbf{u} Y_F) = \nabla.(\rho DF\nabla Y_F) + \frac{A}{F}Y_F Y_o exp\left(-\frac{T_a}{T}\right) \tag{2.54}$$

ere Y_F is the fuel mass fraction, $\rho D\nabla Y_F$ is the molecular diffusion flux, and $AY_F Y_o exp\left(-\frac{T_a}{T}\right)$ represents the instantaneous reaction rate $\dot{\omega}$, where A is an exponential factor, and T_a is the activation temperature.

The inclusion of F in the governing equations changes the relation between the physical and chemical timescales, due to which the turbulence-chemistry interactions are altered. One possible method to resolve this issue is through introducing a field variable G to track the flame front position [68], but the governing equation for G includes the turbulent flame speed S_T, which does not have a universally accepted closure model. Owing to this limitation, the TFM model is developed using another approach called the flame-surface density analysis [69].

The flame-surface density analysis assumes a Lewis number (Le) equal to 1, which means that the mass and thermal diffusivities respectively are equal. This assumption leads to a linear relationship between reactive species mass fractions and temperature, and both can be linked through reaction progress variable c. The value of c lies between 0 and 1, with c = 1 signifying a fully burnt mixture while c = 0 indicating an unburnt reactant mixture. As a result, the fuel-mass balance equation described above is altered as follows,

$$\frac{\partial \bar{\rho}\tilde{c}}{\partial t} + \nabla.(\bar{\rho}\tilde{\boldsymbol{u}}\tilde{c}) + \nabla.\left[\left(\bar{\rho}(\widetilde{\boldsymbol{u}c} - \tilde{\boldsymbol{u}}\tilde{c})\right)\right] = \overline{\nabla.(\rho D \nabla c)} + \overline{\dot{\omega}_c} \qquad (2.55)$$

where the quantities with tilde are mass-weighted filtered and the quantities with bar are LES-filtered quantities. The right-hand side of the equation can also be represented in terms of flame front displacement as follows,

$$\overline{\nabla.(\rho D \nabla c)} + \overline{\dot{\omega}_c} = \overline{\rho w |\nabla c|} \qquad (2.56)$$

while the flame front displacement term can also be expressed as,

$$\overline{\rho w |\nabla c|} = \langle \rho w \rangle_s \Sigma = \Xi |\nabla \bar{c}| \qquad (2.57)$$

where $\langle \rho w \rangle_s$ is the mass-weighted displacement speed, Σ is subgrid scale flame surface density, and Ξ is the subgrid scale flame wrinkling factor.

2.4 Reaction Kinetics in Combustion Modelling

The accuracy of any combustion analysis is significantly dictated by the level of detail with which the reaction kinetics are incorporated. A combustion process realistically consists of several reaction steps consisting of different species, each with distinct reaction rates that are nonlinear functions of physical and chemical parameters. However, the need for reduction of the computational cost of such analyses requires a simplification of the reaction kinetics. The simplest way to do so is to assume fast (one-step) chemistry, in which the reactants are

instantly oxidized without any intermediary reaction steps. While this approach suits relatively simpler numerical setups, more complex setups require a greater level of detail to capture the flow dynamics more accurately. For such cases, there exist reaction kinetic mechanisms that are significantly reduced from the detailed mechanisms but incorporate a greater level of detail compared to fast chemistry [11]. Another approach involves the determination of species distribution through joint probability density functions (PDFs) of a normalized variable called mixture fraction (covered in detail in the later sections). The choice of chemical kinetic mechanism depends on the complexity of the computational setup as well as the turbulence and combustion models respectively.

2.5 Chemical Kinetic Mechanisms

Chemical kinetic mechanisms play a major role in dictating the distribution of species and the temperatures in the computational domain. For the determination of reactive flow dynamics, transport equations take into account the chain of chemical reactions and reaction rate constants, the complexity of which depends on the availability of computational resources. These mechanisms include vital information about the species involved, their reactions, and the associated rate constants. Coupled with the models for turbulence-chemistry interactions, these kinetic mechanisms are used to forecast the course of combustion, including the distribution of chemical species and the temperature profile inside the combustion chamber, by using this data as input for computational models. These kinetic mechanisms range from relatively simpler global mechanisms to complex detailed mechanisms that contain a long chain of reactions to encapsulate the combustion process. Some notable chemical mechanisms used in numerical studies of the dual swirl partially premixed combustion are reviewed in the next subsections. Table 2.2 shows the full list of the chemical kinetic mechanisms utilized in these numerical validation analyses.

2.5.1 Global Mechanisms

To reduce the computational time of the combustion-related simulations, various global mechanisms have been derived over the years that range from 1-step to 5-step reactions respectively. While recent studies have seen an increase in the complexity of chemical mechanisms being utilized, global mechanisms were frequently employed in earlier studies owing to the higher computational cost associated with detailed mechanisms.

Major global mechanisms developed over the years for methane-air combustion include two distinct 3-step mechanisms [70] [71] that include 5 species (CH_4, CO_2, CO, O_2 and H_2O), another mechanism consisting of the aforementioned 5 species, but having 2-steps and different reaction rates [72] and, a 3-step mechanism [73] that includes 6 species (CH_4, CO_2, CO, O_2, H_2, and H_2O). Along with the number of reaction steps, each of these chemical kinetic mechanisms have different reaction rates for each reaction.

A "tuned" 5-step global mechanism was proposed to improve the accuracy of the previously developed chemical mechanisms in addition to predicting the formation of NO [11]. The model is an extension to the previously proposed 3-step reaction mechanism [71] but has different reaction rates. This model also offered an alternative to the prediction of NO formation through lookup tables in post-processing [74].

2.5.2 Detailed chemistry and reduced detailed mechanisms

GRI Mech is one of the most commonly utilized detailed chemical mechanisms in combustion-related simulations, and as per the author's findings, all validation studies of dual swirl partially premixed combustion covered in this review that employed detailed chemistry used GRI Mech as the chemical kinetic mechanism. So far, 3 versions of this mechanism have been released, and GRI Mech 3.0, [75] the most recent one, includes 53 species and 325 elementary reactions that capture the hydrocarbon oxidation process in combustion simulations.

The reduced detailed mechanisms offer greater complexity than the global mechanisms but are not as computationally intensive as the detailed mechanisms. These reduced mechanisms include used DRM22 [76], a reduced form of GRI Mech 2.11, that contains 22 species and 104 reactions. Another such mechanism is ARM2, [77], a reduced mechanism that contains19 species and 15 reactions.

Chapter 3: LITERATURE REVIEW

Gas turbine combustors have the utmost importance in the aviation industry, as they are used to power the aero engines for thrust generation. Increasing air traffic over the years has continued to raise environmental concerns, as the gas turbine emissions contain harmful combustion byproducts like CO and NOx [1], due to which various regulations have been passed to limit the emission of pollutant gases. To keep in line with the ever-updating regulations limiting the harmful aero emissions, gas turbine combustion technology has also experienced continuous upgrades and modifications over the years. One such approach that is lean combustion [3]. While lean combustion reduces the concentration of NOx and CO in the emissions, it also leads to instabilities in the combustion process like blowoff [4][5] and thermoacoustic oscillations [6][7], which are caused by inefficient mixing due to deviation from stoichiometric ratio. One of the methods to overcome the problem of inefficient mixing in lean combustion is the introduction of components that ensure quick, efficient mixing, like swirlers, which impart angular momentum to the incoming stream of air, leading to rapid mixing between the reactants upon entering the chamber. The DLR dual swirl gas turbine combustor, [8][9] the geometry of which will be utilized in this study, is an example of such a configuration. The flow behaviour resulting from such configuration resembles that of a premixed combustor configuration despite the DLR GT combustor having the build of a non-premixed combustor barring the swirlers, due to which the combustion taking place is referred to as partially premixed.

This chapter mainly covers the numerical validation studies featuring flow analysis of the dual swirl partially premixed combustion chamber domain using different boundary conditions and scopes of analysis. The overview of the numerical validation case studies will be preceded by an overview of the experimental study by DLR based on which the numerical analyses were conducted.

3.1 Benchmark experimental case study

The numerical validation case studies covered in this literature review are based on the experimental study conducted in a dual-swirl GTMC. The study, divided into two parts, analyzed 3 distinct CH4/air diffusion flame types that are differentiated based on their stability.

The first part of the experiment covers the flow features, temperature, and species distributions respectively, while the second part focuses on the turbulence-chemistry interactions.

The experiment was conducted using non-invasive optical methods, which included Laser Doppler Velocimetry (LDV) for obtaining flow velocities at various heights, laser Raman spectroscopy for mixture fractions, species mass fractions, and temperature measurements respectively, Particle Image Velocimetry (PIV) for obtaining instantaneous flow fields on selected mid-planes, and Planar Laser Induced Fluorescence (PLIF) for the measurement of OH radicals. These measurement techniques were facilitated by the transparent chamber design.

The combustor features a square cross-section chamber of 85x85 mm and a height of 114 mm, which is walled on all sides by quartz plates that allow for the optical measurement techniques to be employed. The walls are supported by steel posts at the corners. There are three inlets to the chamber, two of which are air inlets, while the third one is for CH_4. Dry air enters the combustor at room temperature via a plenum, which keeps the air and CH_4 segregated before they enter the chamber. The airflow is divided in the plenum to be passed through 2 radial swirlers, which lead to the central and annular inlet nozzles respectively. The central nozzle is 15 mm in diameter, while the annular nozzle has inner and outer diameters of 17mm and 25 mm respectively. The swirlers leading to central and annular nozzles consist of 8 and 12 channels respectively. The air mass-flow ratio of annular swirler to central swirler is approximately 1.5. The fuel nozzle lies between the two air nozzles, to which non-swirling fuel

is supplied through a total of 72 channels, each one having a square cross-section of 0.5 x 0.5 mm. The combustor schematic is shown in **Figure 3.1**.

3.2 Overview of the investigated experimental cases

The benchmark DLR dual swirl experiment investigated 3 cases called Flames A, B, and C respectively. All three flames were operated in globally lean conditions to observe the
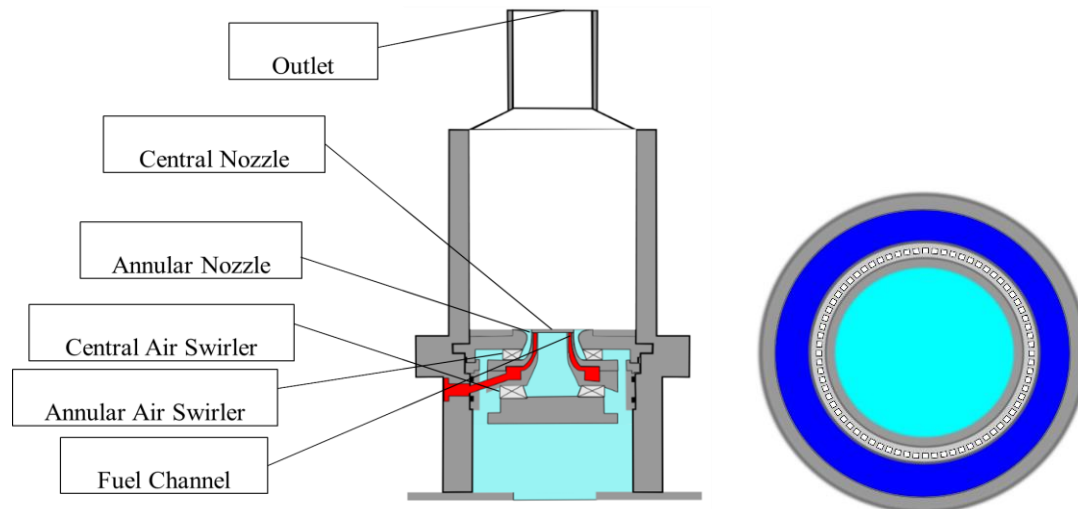

Figure 3.1: 2D schematic diagram of the DLR dual-swirl combustion chamber (left) and top view of the inlet nozzles with fuel channels (right)

reduction in the emission of pollutants. Flame A displayed stable characteristics overall, while Flames B and C were observed to be distinctly unstable. Common features like V-shaped toroidal flame structures and zones dominated by reverse-flow called recirculation zones in the central and near-wall regions respectively were observed in all 3 cases, while no soot formation was observed in either case.

The recirculation zone observed in the central part of the chamber is referred to as the inner recirculation zone (IRZ) while the corresponding near-wall zone is called the outer recirculation zone (ORZ), which occurred in the lower corners of the chamber. Recirculation zones contribute towards stabilizing the flame by transporting the hot gases towards the fresh stream of incoming propellants, thereby reducing the reaction time for the combustion to occur. Each recirculation zone was separated from the normal flow by a "shear layer" where the mean axial velocity, u was observed to be 0 m/s. The shear layers were also observed to be the regions where reaction rates were the highest in all 3 cases, and were physically characterized by the flame opening angles. The flame operating near lean blowout conditions (equivalence ratio $\Phi_{glob} = 0.53$), which is the focus of this study, was called "Flame C" in the

experimental investigation, and was characterized by the periodic liftoff of the flames, followed by a period of stable burning. The distinct liftoff behaviour of the flames compared to the stable flame was proven by the similar distribution but significantly lower concentration of the CH and OH particles in reaction zones. The blowoff behaviour of the flames led to the mean equilibrium temperature in this case being the lowest of the 3 cases investigated. The flame characteristics of all three flames are shown in **Table 3.1**.

3.3 Numerical case studies differentiated by combustion model

In this section, the numerical validation studies of the DLR dual swirl partially premixed experimental studies will be discussed in order of the combustion models used.

3.3.1 Eddy Dissipation Concept

Multiple studies have employed the Eddy Dissipation Concept (EDC) for analyzing the thermochemical behaviour in a dual swirl partially premixed configuration.

Table 3.1: Characteristics of the 3 cases investigated in the DLR dual swirl experimental study

Case	Distinct characteristic	Flow Rates (g/min)		Φ_{glob}	Mean IRZ height (mm)	Jet Opening Angle $\frac{\theta}{2}$ (degrees)	Mean equilibrium temperature (K)
		Air	Fuel				
Flame A	Stable flame	1095	41.8	0.65	70	≈30	1750
Flame B	Thermoacoustically unstable flame	281	12.3	0.75	62	75	1915
Flame C	Liftoff and flashback	281	9.0	0.55	72	≈30	1500

These numerical validation studies have combined EDC with a variety of turbulence models and chemical kinetic mechanisms, like RANS k-ε coupled with a 2-step reaction mechanism [78][79], RANS-RSM coupled with DRM22 chemical kinetic mechanism [80], RANS k-ε coupled with DRM22 chemical kinetic mechanism [81] LES coupled with a 3-step

reaction mechanism [82]. All these studies analyzed the stable flames in a partially premixed environment, and while they predicted the flow features and temperature fields with reasonable accuracy, the near-inlet predictions using the EDC model depicted considerable deviation from experimental data as compared to the predictions at downstream regions. Another observation made from these studies is that the use of detailed chemical kinetic mechanisms like DRM22 along with EDC gives a considerably higher accuracy for near-inlet predictions compared to the simpler global mechanisms.

3.3.2 Flamelet/Progress Variable Approach

As per the author's knowledge, the FPV model is the most extensively utilized combustion model in the dual swirl partially premixed numerical studies and has proven to have a relatively higher accuracy level compared to the other combustion models. It has been coupled along with URANS and LES turbulence models [82] to produce reasonable results in a comparative study of different turbulence and combustion models. Another study [83] employed 2 different variations of FPV model called F-Cvar [84] and F-TACLES [85] [86]. F-Cvar includes the progress variable variance in the system of equations while solving for the scalars, while F-TACLES introduces a flame wrinkling factor by generating a flamelet library consisting of 1D premixed stratified flamelets. The results of the study showed that both F-Cvar and F-TACLES achieved slightly higher accuracy compared to FPV. Further studies coupled the LES and FPV models to observe stable flame behaviour [87], thermoacoustically unstable flame properties [88], as well as the effects of the exclusion of the fuel plenum in the computational domain [89], with the results showing that the inclusion of fuel plenum produced more accurate results. Another study analyzed the influence of the PVC on flame dynamics for both stable and thermoacoustically unstable flames using FPV and LES [90], while the same models were employed to predict the behaviour of a flame close to the blowoff limit [39], and the effects of introducing different heat-loss effects to the flame close to blowoff [91], which showed that introducing heat loss through heat loss factor κ [92] resulted in a more unstable flame behaviour compared to the adiabatic case. A fairly recent study [93] applied reduced order modelling to reduce the computational time of a case simulated initially using the FPV-LES models, while another study analyzed the influence of PVC on the dynamics of a flame close to blowoff [94].

3.3.3 Eddy Dissipation Model

As per the author's knowledge, there exist three studies that have utilized the Eddy Dissipation Model-Finite Rate Chemistry (EDM-FRC) model to simulate dual-swirl partially premixed combustion. As mentioned in the previous chapter, the utilization of EDM with FRC is important as it helps overcome the limitation of the EDM model by predicting the thermochemical behaviour better in regions where chemical time scales dominates. This model has been used with the Scale Adaptive Simulation (SAS) turbulence model, which is a RANS-LES hybrid, along with a one-step chemical mechanism to simulate stable flames [95] as well as flames close to blowoff [96]. Another study utilized EDM-FRC along with the URANS k-w and DES turbulence models while employing a 3-step chemical mechanism [23], with all 3 studies achieving reasonable accuracy.

3.3.4 Flamelet Generated Manifold

As per the author's knowledge, there exist three numerical analyses of the dual swirl partially premixed combustion that have utilized the FGM combustion model. One study used FGM along with the URANS-RSM and DES turbulence models [97], in which DES predictions were generally more accurate. A couple more studies [98] [99] employed a 5-D FGM approach with both RANS and LES models, using GRI Mech 3.0 as the chemical kinetic mechanism. The analysis using LES compared a fully adiabatic approach with two different heat loss approaches, in which the fully adiabatic model gave more accurate thermochemical predictions compared to the models incorporating heat losses.

3.3.5 Conditional Moment Closure

The only dual swirl partially premixed numerical study utilizing the LES-CMC approach validated the flame close to blowoff by employing the ARM2 reduced detailed chemical mechanism [100]. With the exception of velocity profiles near inlet, the model showed a high level of accuracy in its prediction of flow dynamics and thermochemical features.

3.3.6 LES-Thickened Flame Model

As per the author's knowledge, there is a singular numerical analysis of the dual swirl partially premixed combustion that utilized the LES-TFM model [101]. The study aimed to reduce the flame thickening due to TFM in regions of low heat release, which caused the

reaction rates to be abnormally high in those regions. To overcome this issue, 4 different sensors were introduced to reduce flame thickness in regions of low reactivity via detection of a flame parameter. Among those sensors, the "Chemical Explosive Mode Analysis" (CEMA) sensor [102] predicted the thermochemical parameters with the highest accuracy. An optimized version of CEMA was used in this study to reduce the computational cost of the analysis, since CEMA is more intensive than other sensor models.

3.4 Numerical case studies differentiated by chemical kinetic mechanism

All global chemical schemes have been derived from the elementary one-step methane-oxygen combustion equation, which, as per the author's knowledge, multiple numerical studies analyzing dual swirl partially premixed combustion have utilized [95] [103]. The mechanism is represented by the following reaction.

$$CH_4 + 2O_2 \rightarrow CO_2 + H_2O \tag{3.1}$$

A three-step chemical kinetic mechanism was employed for the numerical investigation of the partially premixed case close to blowoff [104]. This global mechanism utilized the 5-step mechanism [11] with the omission of the reactions involving the NO species.

$$CH_4 + \frac{3}{2}O_2 \rightarrow CO + 2H_2O \tag{3.2}$$

$$CO + \frac{1}{2}O_2 \rightarrow CO_2 \tag{3.3}$$

$$CO_2 \rightarrow CO + \frac{1}{2}O_2 \tag{3.4}$$

A 2-step irreversible chemical kinetic scheme derived from a mechanism consisting of 5 species [105] was used to numerically validate the DLR experiment [23]. A few validation studies [103] [79] utilized the same mechanism but considered the second reversible reaction as irreversible.

$$CH_4 + \frac{3}{2}O_2 \rightarrow CO + 2H_2O \tag{3.5}$$

$$CO + \frac{1}{2}O_2 \leftrightarrow CO_2 \tag{3.6}$$

Another validation study [82] utilized a 3-step mechanism by breaking down the reversible reaction in this scheme into 2 separate reactions.

As per the author's knowledge, a majority of the recent numerical validation studies of dual swirl partially premixed combustion [99][39][94] have employed GRI Mech 3.0 as the chemical kinetic mechanism. Some numerical validation studies have also utilized the predecessors of Gri Mech 3.0, like Gri-Mech 2.11 [106], and Gri-Mech 12 [107].

Among the studies that utilized the reduced detailed mechanisms, one study [80] used DRM22 [76] for the 2D analysis of Flame A using EDC and RANS-RSM as the combustion and turbulence models respectively. Another study [100] numerically validated the of the DLR experiment utilizing ARM2 [77], while another numerical analysis of the DLR experiment [101] used a reduced skeletal mechanism developed using in situ adaptive tabulation [108][109] that contained 16 species and 41 reactions.

3.5 Comparative overview of the case studies

Among the numerical validation analyses consulted for this literature review, most of the case studies analyzed the stable-burning "Flame A", and it was noted that the flow dynamics like axial, radial, and swirl velocities respectively, were captured with considerable accuracy by the studies utilizing the LES turbulence model due to its resolution of the large scale eddies. An especially crucial region in the computational domain for these analyses was the near-inlet zone, where the largest discrepancies were noted in the axial velocity predictions. The LES-based studies predicted the flow development in this region with the highest accuracy. Similarly, the highest levels of accuracy for temperature predictions were observed in studies utilizing the LES-based models, with the LES-FPV [88][89][90] studies remaining consistently accurate in downstream predictions as well.

Almost all numerical analyses of "Flame B" and "Flame C" were conducted using the LES-FPV turbulence model, with the exceptions of the "Flame C" analysis by Rebosio et. al [96], which utilized the SAS-EDM-FRC models, and LES-CMC analysis by Zhang and Mastorakos [100]. It was noted that while all analyses of "Flame C" achieved high accuracies in capturing near-inlet axial velocities, the SAS-EDM-FRC analysis significantly overpredicted the temperatures close to inlet nozzles as compared to the LES-FPV studies, which achieved reasonable accuracy levels [39][91].

It was also noted that the studies utilizing detailed kinetic mechanisms and reduced detailed mechanisms generally achieved a greater level of accuracy compared to those that utilized global reaction schemes with limited number of species and reaction steps. The list of numerical validation analyses consulted for this literature review are summarized in **Table 3.2**, **Table 3.3** and **Table 3.4**.

3.6 Research gap based on literature review

From the overview of the case studies, it was determined that no numerical analysis has been conducted for "Flame C" using the DES tubulence model and the EDC combustion model. Another major observation was that no study of "Flame C" performed a parametric analysis comparing varying geometry. Based on this observation, the scope of this study, which consists of a validation analysis using the DES-FPV and DES-EDC models, as well as a parametric analysis featuring the effects on flow dynamics of varying swirler angles, was defined.

Table 3.2: Numerical Analyses of the "Flame A" case of the DLR experimental study

Combustion Model	Turbulence Model	Chemical Mechanism	References
EDM-FRC	SAS	One-step mechanism	Widenhorn et al. (2009) [95]
	RANS (RSM)	One-step mechanism	Sudarma and Morsy (2018) [103]
	URANS-k-w, DES	Three-step mechanism	Ben Sik Ali et al. (2016) [23]
EDC	RANS-k-ε	Two-step mechanism	Bahramian (2015), Bahramian et al. (2017) [78] [79]
	RANS (RSM) (2D grid)	DRM22	Mardani & Fazlollahi-Ghomshi (2016) [80]
	LES	Three-step mechanism	Benim et al. (2017) [82]

	RANS-k-ε	DRM22	Mardani et al. (2022) [81]
FGM	URANS (RSM), DES	GRI Mech 3.0	Wankhede et al. (2014) [97]
	RANS-k-w	GRI Mech 3.0	Donini et al. (2015) [98]
	LES	GRI Mech 3.0	Donini et al. (2017) [99]
TFM	LES	Reduced Skeletal Mechanism	Zhang et al. (2021) [101]
FPV	URANS (SST), LES	Three-step mechanism	Benim et al. (2017) [82]
	LES	GRI Mech 2.11	See & Ihme (2015) [83]
	LES	GRI Mech 3.0	Z. X. Chen, Swaminathan, et al. (2019) [88]
	LES	GRI Mech 3.0	Z. X. Chen & Swaminathan (2020) [89]
	LES	GRI Mech 3.0	Z. X. Chen, Langella, et al. (2019) [90]
	LES	GRI Mech 2.11	D. Huang et al. (2020) [87]
	LES	GRI Mech 1.2	Arnold-Medabalimi et al. (2022) [93]

Table 3.3: Numerical Analyses of the "Flame B" case of the DLR experimental study

Combustion Model	Turbulence Model	Chemical Mechanism	References
FPV	LES	GRI Mech 3.0	Z. X. Chen, Swaminathan, et al. (2019) [88]

Combustion Model	Turbulence Model	Chemical Mechanism	References
			Z. X. Chen & Swaminathan (2020) [89]

Table 3.4: Numerical Analyses of the "Flame C" case of the DLR experimental study

Combustion Model	Turbulence Model	Chemical Mechanism	References
EDM-FRC	SAS	Two-step mechanism	Rebosio et al. (2010) [96]
CMC	LES	ARM2	H. Zhang & Mastorakos (2019) [100]
FPV	LES	GRI Mech 3.0	Massey et al. (2019) [39], Massey et al. (2021) [91], Massey et al. (2022) [94]

Chapter 4: METHODOLOGY

Numerical analysis of turbulent combustion requires multiple factors to be taken into consideration, due to which the preparation of the computational setup relies not only on the knowledge of numerical modelling, but also of the various features of the flow dynamics that can be obtained in post-processing. There are different routes which can be taken during post processing in terms of the type of data that needs to be obtained, which defines the scope of the analysis.

Based on the diverse scope of numerically setting up a turbulent combustion problem as well as the focus of the research being driven by the flow features to be studied, the research gap in a turbulent combustion analysis can be based on either of these factors. The numerical setup itself is divided into three categories, which are, as mentioned in the previous chapters, the turbulence model, the combustion model, and the chemical kinetic mechanism. The various factors based on which the novelty is sought in any combustion-related analysis is shown in figure 4.1. This chapter provides an overview of the approach taken to discover the research gap, based on which the numerical setup and the scope of the results was determined.

4.1 Review of the case studies

As seen in the previous sections, there exist multiple numerical analyses of dual swirl partially premixed combustion, and each of these studies explicitly specify the inlet conditions and numerical models employed in the analysis. Among all the numerical validation studies of the DLR dual swirl experimental analysis [8][9], most have performed validation of the stable combustion case, while there are also a few studies analyzing the thermoacoustically unstable flames. Among the numerical validation analyses that investigated lean flames close to blowoff, it was observed that all but one of those studies utilized LES as the turbulence model, while the other remaining study used the RANS-LES hybrid Scale Adaptive Simulation (SAS) [96] model. Similarly, Flamelet/Progress Variable [91] [39] [94] approach was the most commonly utilized combustion model, while the other two models utilized in these studies were Eddy Dissipation Model (EDM) [96] and Conditional Moment Closure (CMC) [100].

Based on the numerical setup utilized in these studies, and considering the high level of accuracy associated with the FPV approach compared to other models, a reasonable research approach was to test the accuracy of the FPV model by coupling it with the Detached eddy

simulations (DES) turbulence model, which presents a trade-off in terms of lower accuracy and greater computational efficiency compared to the LES model. It was also noted that all the numerical studies based around lean unstable partially premixed combustion utilized a solitary combustion model to analyze the flow behaviour, and none of those studies had, despite its extensive usage in the earlier studies of stable flames, utilized the eddy dissipation concept. (EDC) combustion model. Based on this observation, it was decided to compare the results of both the FPV and the EDC models for this study.

All of the numerical validation studies of lean partially premixed flames focus on both the turbulence-chemistry interactions as well as the influence of the pressure-induced vortex on the flow dynamics. However, it was noted that none of the studies analyzed the changes in the behaviour of reactive flow due to variations in the swirler geometry, based on which an additional analysis was to be performed to observe changes in the flow and thermochemical behaviours respectively with increasing swirler angles. A similar study was conducted for stable flame analysis [81] using EDC, but it varied multiple parameters at a time due to which the dependence of flow behaviour solely on increasing swirler angles couldn't be distinguished.

4.2 Numerical Setup

4.2.1 Computational Domain

The computational domain of the dual swirl partially premixed combustor is shown in **Figure 4.1**, and consists of 3 separate inlets for air and fuel. Air at standard temperature and pressure is introduced from the plenum, and is then divided into two streams, one of which passes through the inner swirler to the central nozzle ($d_i = 15mm$) while the other is transported through the outer swirler to the annular nozzle ($d_i = 17mm$, $d_o = 25mm$ curved to outer diameter of $d_o = 40mm$). The number of inner swirler blades is 8, while that of the outer swirler blades is 12. Fuel is supplied through a peripheral injector consisting of 72 channels, each of which has an area of 0.5x0.5 mm^2. The exit of the annular nozzle is located 4.5mm above the exit of the central nozzle and air inlet. The combustion chamber has a height of 114mm and an area of 85X85mm^2. The diameter of the exhaust outlet is 40mm. The resulting mesh, generated on ANSYS ICEM, consisted of 12.7 million cells.

The swirler assembly of the computational domain for the validation analysis had an inner swirler angle of 60 degrees, while for the parametric analysis, two more domains were generated with inner swirler angles of 62 degrees and 64 degrees respectively.

4.2.2 Boundary Conditions

The boundary conditions for the flow are stated in **Table 4.1**. The mass flow rate of air is 0.00468 kg/s, which is introduced from the air plenum, while that of fuel is 0.00015 kg/s, which is introduced through fuel inlet, as shown in **Figure 4.1**. Both fuel and air enter their respective inlets at the temperature of 298 K. The respective turbulent intensities of air and fuel inlets are 5 percent and 15 percent respectively, while the turbulent length scale for both inlets is 0.0005m.

For the numerical validation analysis, which was performed on *ANSYS Fluent* solver, two separated cases were simulated featuring the Eddy Dissipation Concept (EDC) and Flamelet/Progress Variable (FPV) (Referred to as *Partially Premixed Combustion* on *ANSYS Fluent*) models respectively. As mentioned in the earlier chapters, FPV incorporates joint PDFs of mixture fraction to determine turbulence chemistry interactions, while in the case of EDC, GRI Mech 2.11 chemical kinetic mechanism is employed to integrate the reaction kinetics. For turbulence modelling, Detached Eddy Simulations (DES) is selected, which features both RANS-like and LES-like behaviour based on grid spacing. RANS-like behaviour for DES is modelled through the SST k-ω model. The FPV and EDC analyses were also distinguished on the basis of wall heat transfer, with the FPV analysis employing non-adiabatic and EDC employing adiabatic wall treatment.

4.2.3 Solution

The solution was distributed into 4 phases. The first phase included a short computational simulation of steady, non-reactive flow using the species transport model, following which a transient simulation of non-reactive flow was conducted. Based on the development of the flow dynamics in the transient non-reactive simulations, the reactive simulations were initiated by switching from the species transport model to the prescribed combustion model.

4.2.4 Post Processing and documentation

The post processing phase involved extraction of profiles for different heights along with contours depicting the time-averaged state of the flow as well as the thermochemical properties. The results were then compared with the available experimental data.

Table 4.1: Boundary Conditions for the lean flame numerical analysis

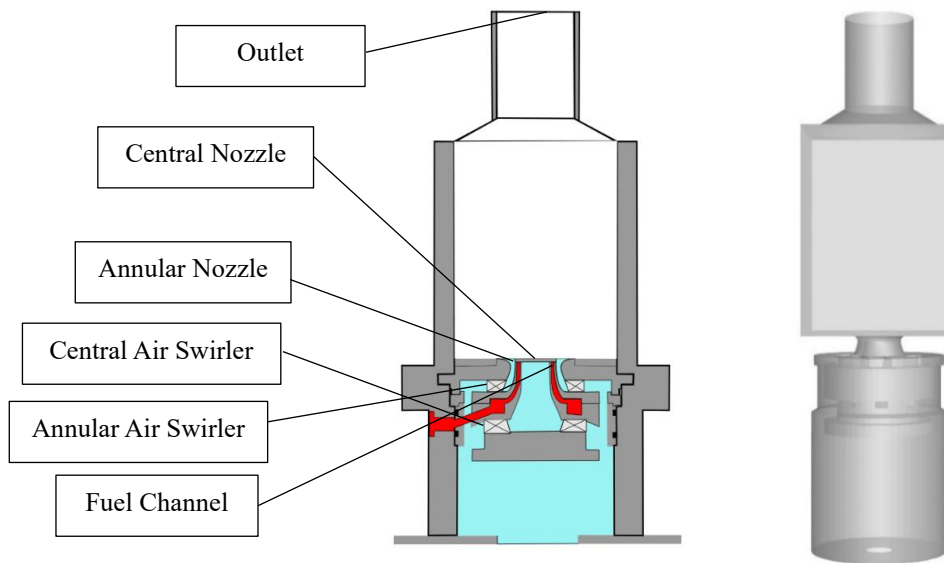| Flow Rates (kg/s)		Φ_{glob}	Boundary Condition		
Air	Fuel		Fuel Inlet	Air Inlet	Outlet
0.00468	0.00015	0.55	Mass-flow inlet	Mass-flow inlet	Pressure outlet

Figure 4.1: 2D schematic diagram of the DLR dual-swirl combustion chamber (left) and 3D computational domain of the combustor (right)
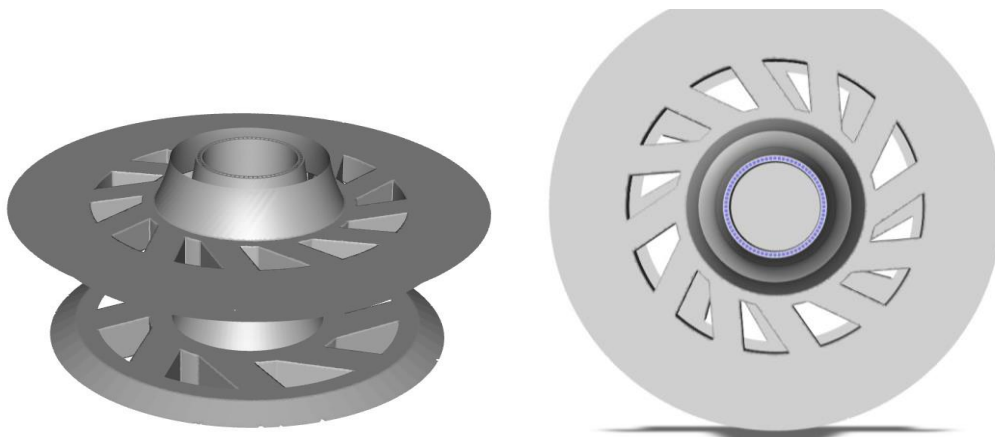

Figure 4.2 Inner and Outer air swirler configuration in the 3D computational domain (left) and top view of the fuel inlet channels (blue) in the swirler assembly (right)
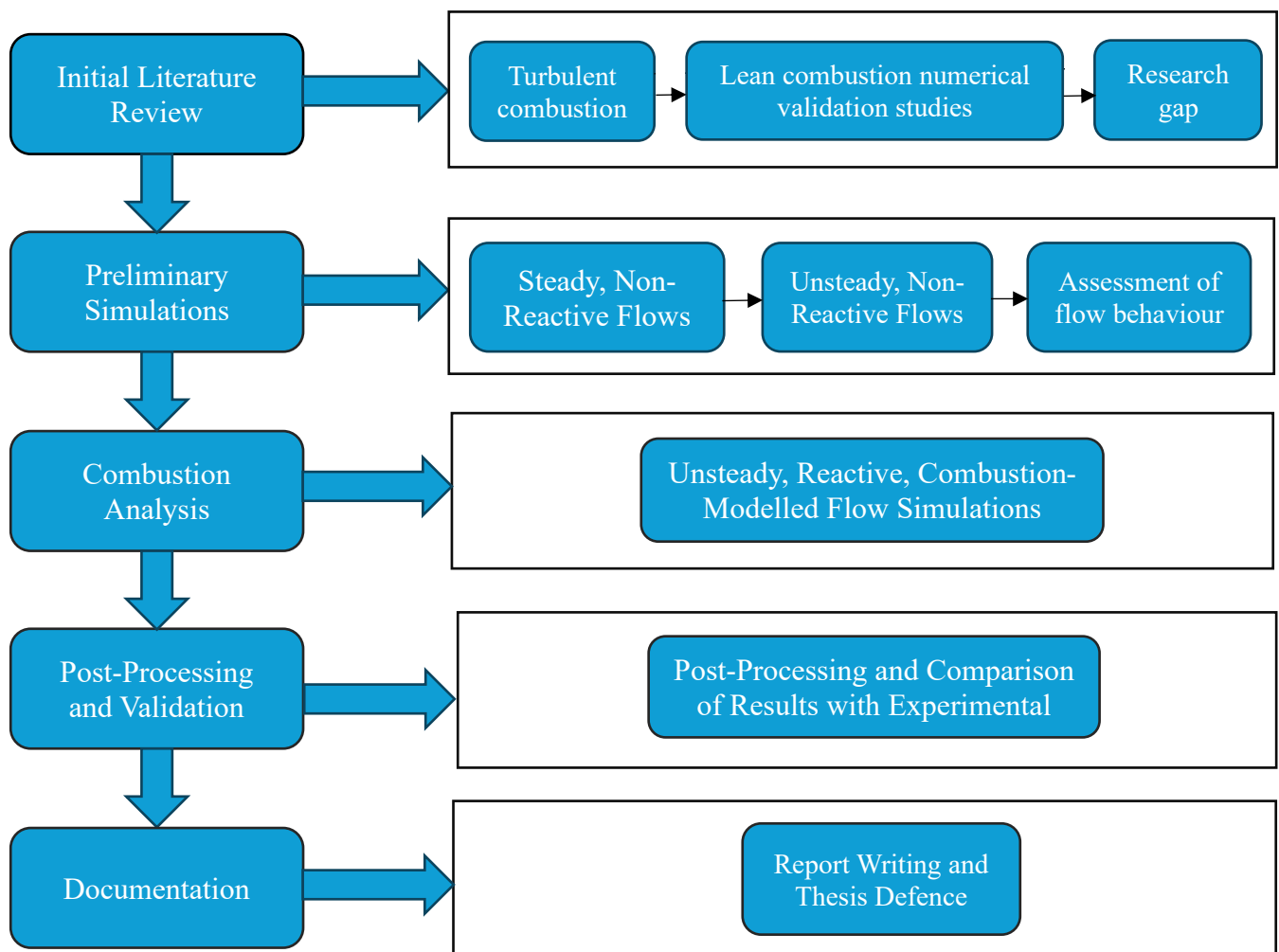
Figure 4.3: Flowchart of the thesis methodology

Chapter 5: RESULTS AND DISCUSSION

This chapter covers the numerical analysis conducted to predict the behaviour of reactive flow. The analysis consists of two parts. 1) A numerical validation study of the DLR dual swirl experimental analysis using two distinct combustion models, and 2) A parametric analysis showcasing the effect of varying the internal swirler angle on the flow dynamics. The first part features a comparison between the *Flamelet/Progress Variable (FPV)* approach using Joint PDFs for species, and the *Eddy Dissipation Concept* (EDC), which utilizes *GRI Mech 2.11* for capturing reaction kinetics. The analysis for the second part was conducted using the *Flamelet/Progress Variable* approach. Both the analyses were conducted using the *Detached Eddy Simulations* as the turbulence model.

5.1 Numerical Validation Analysis with model comparison

The mean axial velocity contours for both the FPV and EDC models can be seen in **Figure 5.1**. In the FPV visuals, there are two distinct recirculation zones on either side of the V-shaped inflow, 1) the inner recirculation zone (IRZ) developed due to the vortex breakdown and 2) the outer recirculation zone (ORZ) formed near the corners of the combustion chamber. "Recirculation zones" are regions of reverse flow which contribute towards stabilizing the flame by transporting the hot gases towards the fresh stream of incoming propellants, thereby reducing the reaction time for the combustion to occur. These recirculation zones are regions of high turbulence and change their size and location rhythmically with time. The recirculation zones are separated from the normal flow by "shear layers" where the mean axial velocity, u was observed to be 0 m/s. The region between the recirculation zones represents the inflow of fresh gas.

The EDC axial velocity contours in **Figure 5.1** show a different shape of the IRZ compared to the FPV visuals. The IRZ shape is significantly flatter and is attached to the chamber base on one side while also having greater width than the IRZ predicted by the FPV model. This shape bears a close resemblance to the "Coanda Flow" [110][111] observed in other similar studies [80][112], which is characterized by the tendency of the flow to stay attached to the surface over which is flows.

The IRZ profiles of both the FPV and EDC models is shown in **Figure 5.2**. It can be seen that the width and height of the FPV profile is overpredicted compared to the experimental
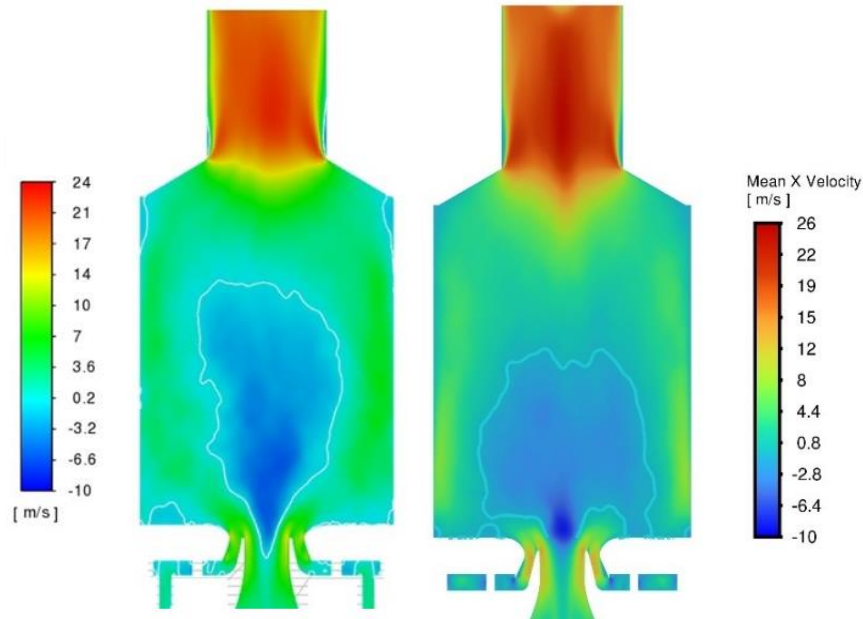
60

Figure 5.1: Time-averaged axial velocity contours for the FPV (left) and EDC (right) models respectively, with IRZ outlines shown

results, while the EDC profile is significantly shorter and wider, while the attachment of the IRZ to the chamber surface can also be clearly seen. This indicates that EDC replicates a much weaker recirculation zone compared to the FPV model.

In **Figure 5.3**, the results of numerically obtained mean axial velocity profiles for the FPV and EDC models respectively are compared with experimental data at different locations of the combustion chamber. The IRZ presence is characterized by negative velocities near the centreline, while the peaks represent the incoming stream of fresh gases. Both FPV and EDC replicate the trends of the experimental results adequately at h = 1mm, but a significant overprediction of IRZ penetration at h = 1mm is quite evident for the EDC model, while a slight underprediction is observed for FPV. This behaviour is quite consistent with that observed in similar numerical studies, which have attributed it to the difficulties in accurately modelling the curvature of the annular nozzle, resulting in such discrepancies in the near-inlet region. For greater downstream locations, FPV predicts the IRZ depth with a significantly greater accuracy compared to EDC, while also replicating the velocity profiles with greater accuracy as compared to the relatively flatter profiles of EDC. However, there is an overall significant underprediction of velocity peaks and an overprediction of IRZ width at all heights.
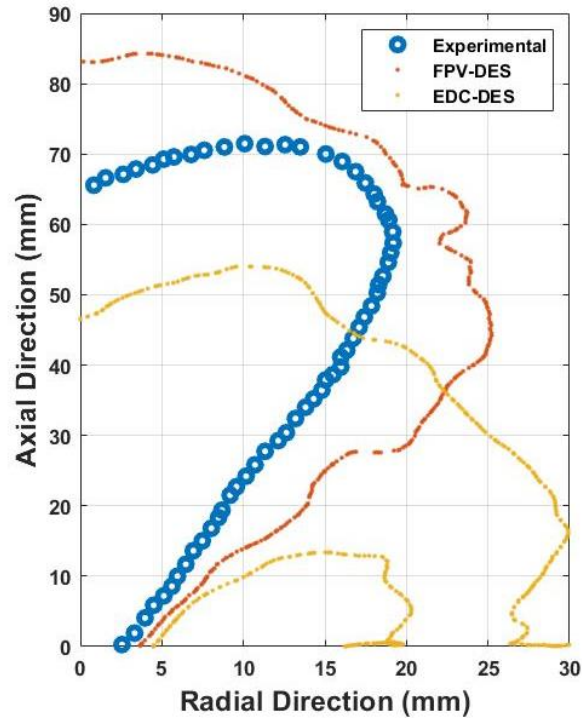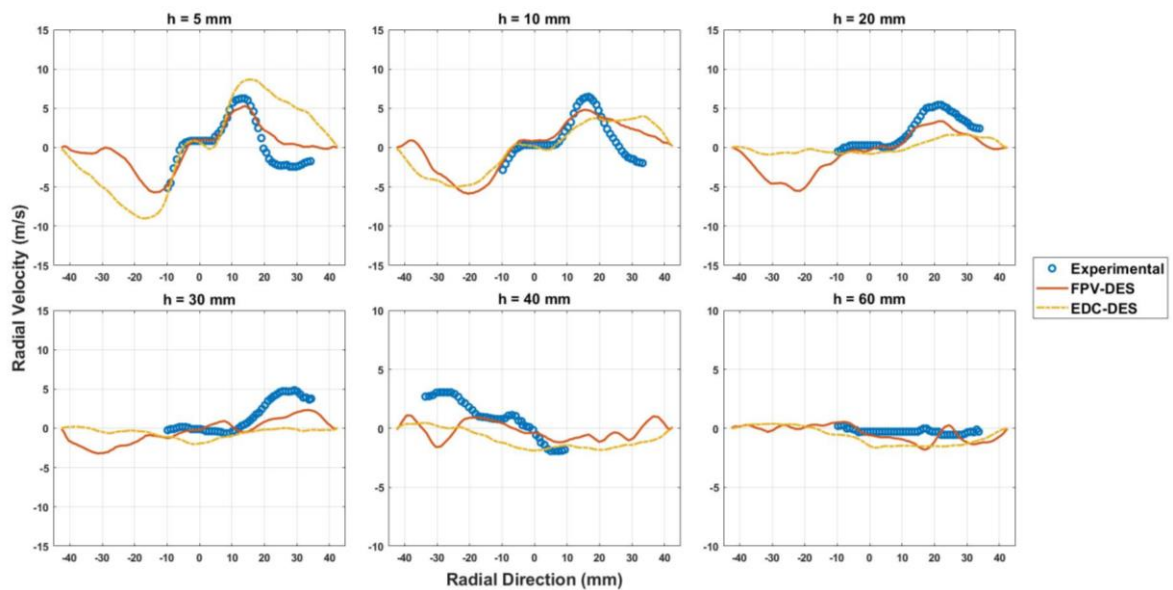
Figure 5.2: IRZ (u=0) isolines for FPV and EDC combustion models compared with the experimental results
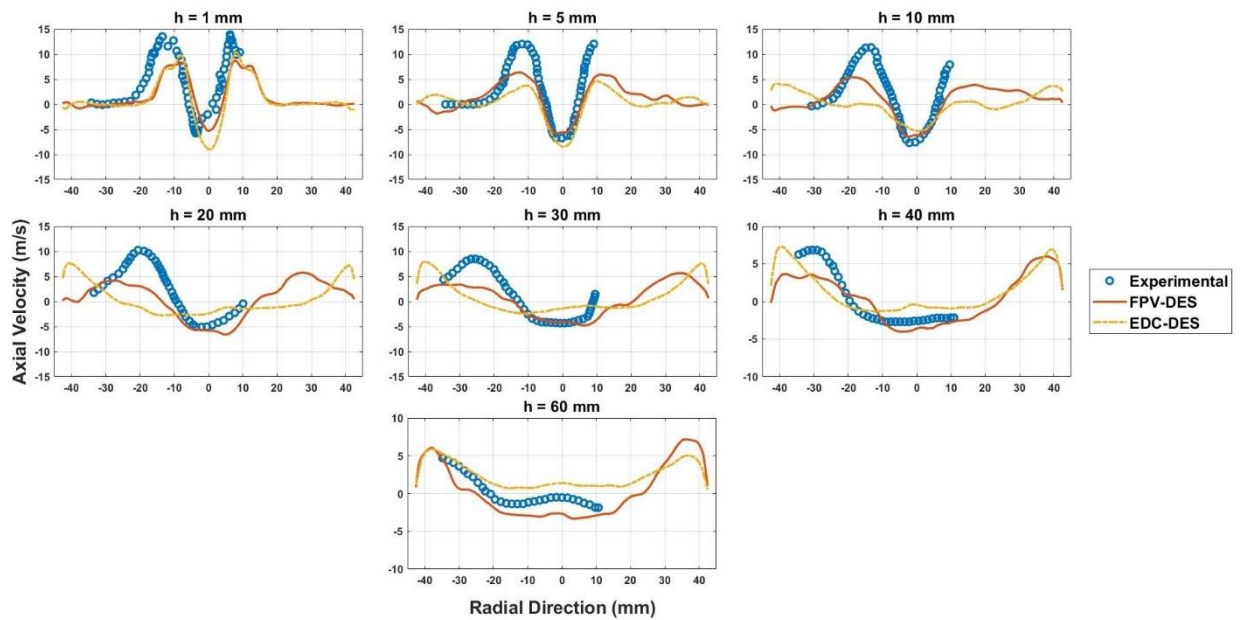
Figure 5.3: Axial velocity profiles for FPV (red) and EDC (yellow) combustion models compared with the experimental result*s*

The radial velocity profiles can be seen in **Figure 5.4**. In the near-inlet region (h = 5mm), both the FPV and EDC models capture the behaviour of the flow with considerable accuracy near the centreline, but show a significant overprediction of near-wall radial velocities at those heights, which implies an underprediction of the ORZ width. The overprediction of IRZ width at greater heights as seen in the axial velocity profiles is evident through the radial velocity profiles as well, with the velocities deviating at downstream heights for both FPV and EDC models respectively. Overall, FPV shows a greater level of agreement with the experimental results compared to the EDC model.

The swirl velocities are shown in **Figure 5.5**. Both models show an underprediction of swirl strength at peak values compared to the experimental results at h =1mm. Generally, FPV shows a better agreement with the experimental values for downstream profiles but owing to its broader and higher IRZ profile compared to that observed experimentally, overpredicts the swirl velocities in the downstream regions.

Figure 5.4: Radial velocity profiles for FPV and EDC combustion models compared with the experimental results
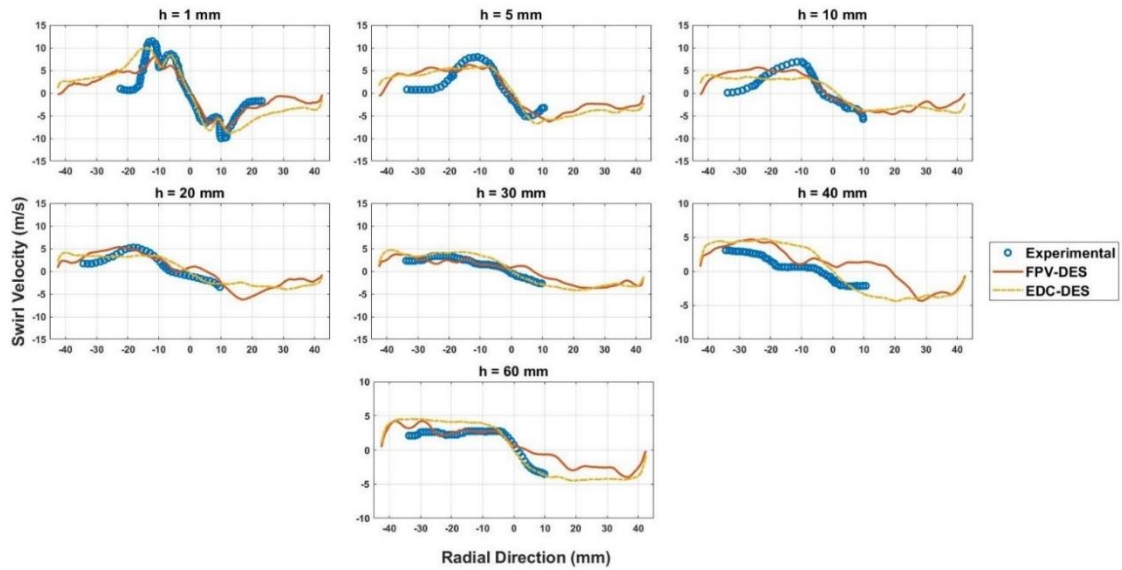
Figure 5.5: Swirl velocity profiles for FPV and EDC combustion models compared with the experimental results

The temperature profiles can be seen in **Figure 5.6**. EDC model significantly overpredicts the temperatures at all heights, while considerable underprediction is seen at the height of 5mm for the FPV model. Both models predict broader peaks for temperature, which is linked to broader IRZ profiles facilitating quick mixing over a greater area compared to the experiment. The experimental data indicates equilibrium temperature (~1450 K) being attained at the height of 10mm, while the FPV results show a significant jump to the equilibrium temperature (~1600 K) between the heights of 10mm and 20mm, which indicates a high reaction rate for the FPV model between those heights, which is confirmed by the sudden disappearance of the mixture fraction peaks and the flattening of the profiles between those heights as seen in the mixture fraction graphs in **Figure 5.7**. Overprediction of temperature and broader profiles at lower height both suggest considerably higher rates of reaction predicted by the EDC model, which is also confirmed by equilibrium being reached at lower heights compared to the experimental results. This conclusion is supported by the CH_4 mass fraction profiles in **Figure 5.8** as well. EDC model shows a significantly high degree of reduction of CH_4 mass fractions by the height of 15mm, and an almost complete consumption of CH_4 by h = 40mm as compared to the experimental results, which indicates quicker reaction rates.

The RMS fluctuation profiles of velocities, depicted in **Figure 5.9**,

Figure 5.10, and **Figure 5.11** show that the FPV case underwent higher transient fluctuations compared to the EDC case. EDC captures the experimental transient fluctuations

of velocities with more accuracy at lower heights compared to FPV. The discrepancy between the two models at capturing the RMS fluctuations is much more evident from the RMS profiles of radial and swirl velocities respectively, which show the FPV case undergoing an overall higher level of fluctuations compared to EDC in the downstream regions as well as in the near-inlet regions for radial velocities.
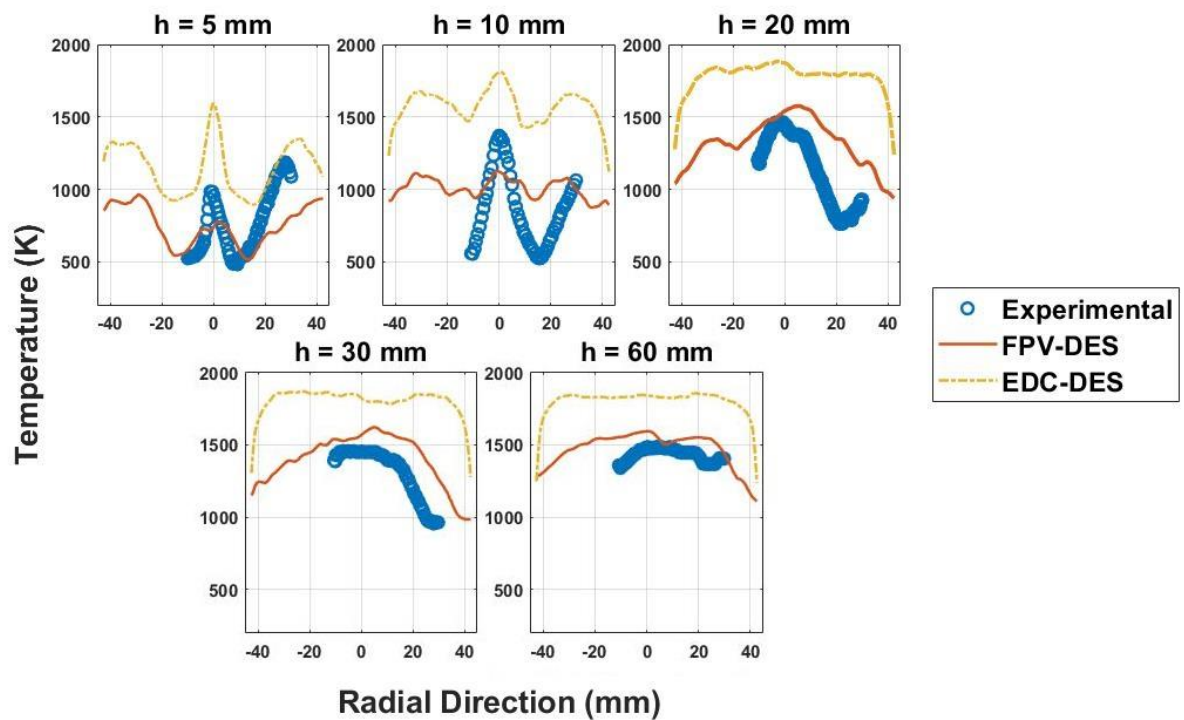

Figure 5.6: Temperature profiles for FPV and EDC combustion models compared with the experimental results

From the temperature RMS fluctuation profiles in **Figure 5.12**, it can be seen that for lower heights, transient fluctuations of temperature are quite high for both models compared to the experimental data, and while there is a reasonable agreement with experimental values for the heights of 20mm and 30mm, the RMS temperature values for both models do not lower down as much as the experimental values for the downstream height of 60mm.
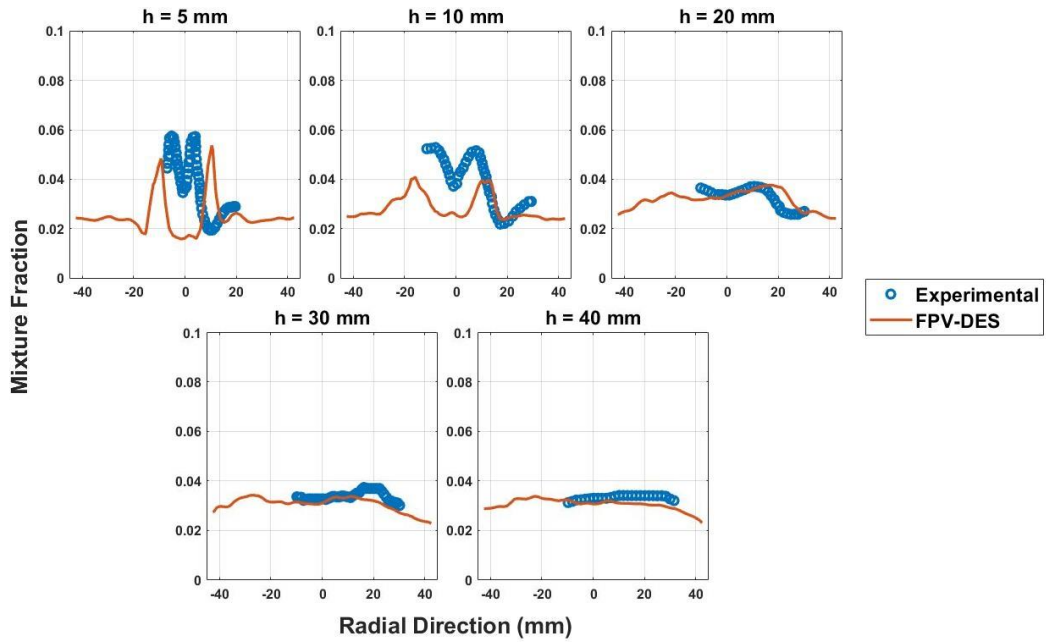
Figure 5.7: FPV mean mixture fraction results compared with the experimental results
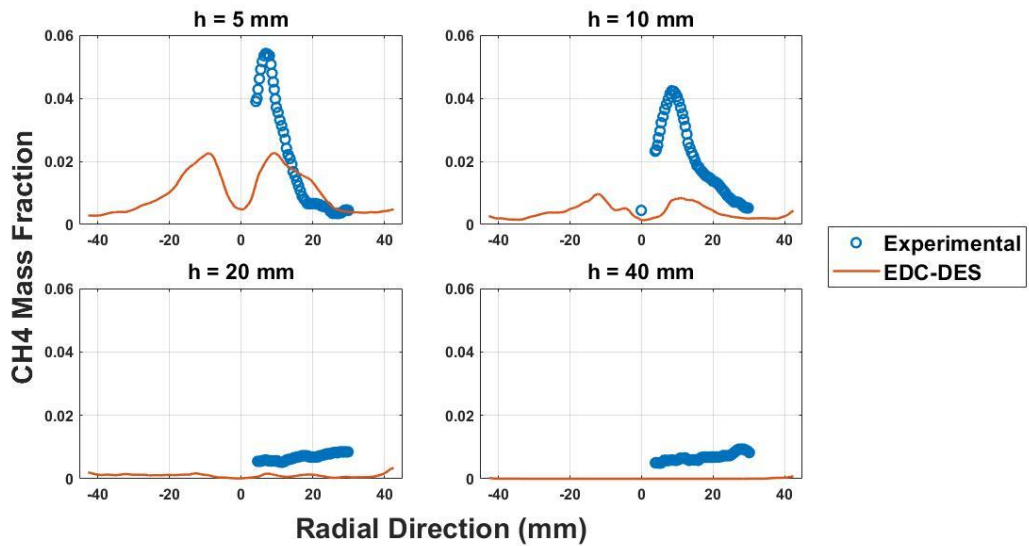
Figure 5.8: CH$_4$ mass fraction profiles EDC combustion model compared with the experimental results

The mean velocity features predicted using the FPV model can be seen from the velocity streamlines shown in **Figure 5.13**. The colour of each line indicates the magnitude of velocity, and the flow behaviour in each zone can be distinguished through the streamlines. The swirling motion of the IRZ is evident in the central region of the pathline diagram, while the V-shaped axial flow outside the IRZ can also be distinguished. **Figure 5.13** also shows the difference
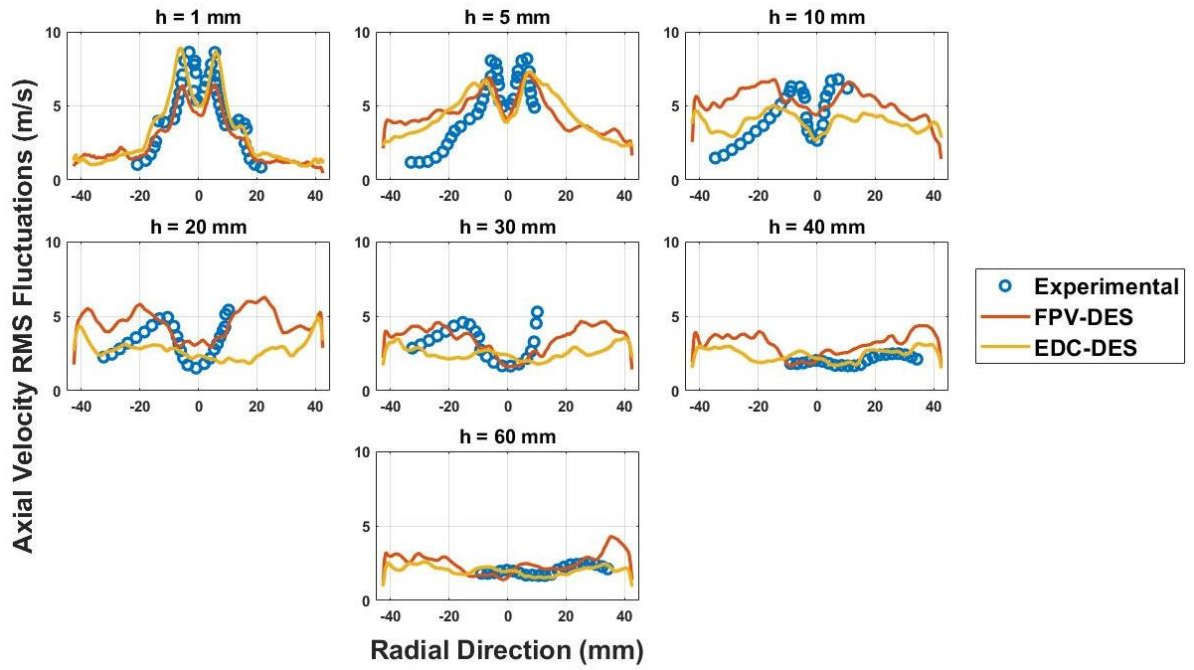
Figure 5.9: Axial velocity RMS fluctuations for FPV and EDC models
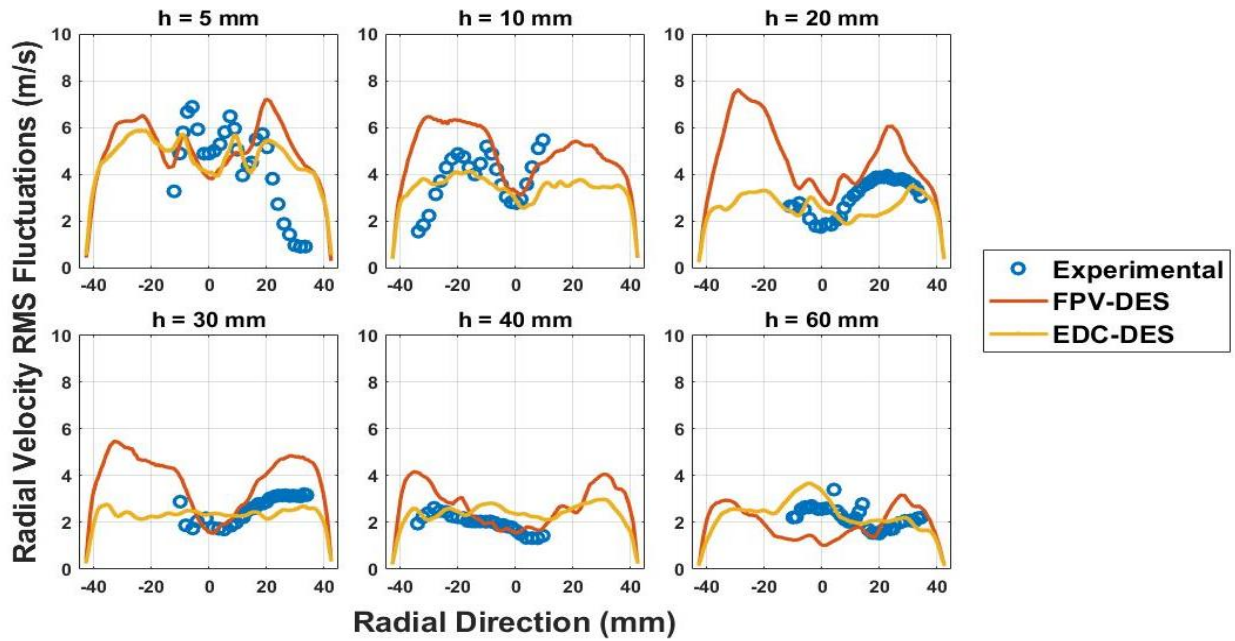
Figure 5.10: Radial velocity RMS fluctuations for FPV and EDC models

between the instantaneous and mean axial velocity fields predicted by the FPV model. The instantaneous contours, which were obtained at an arbitrary time during the simulations, show central swirling regions scattered along centerline instead of a singular IRZ body.
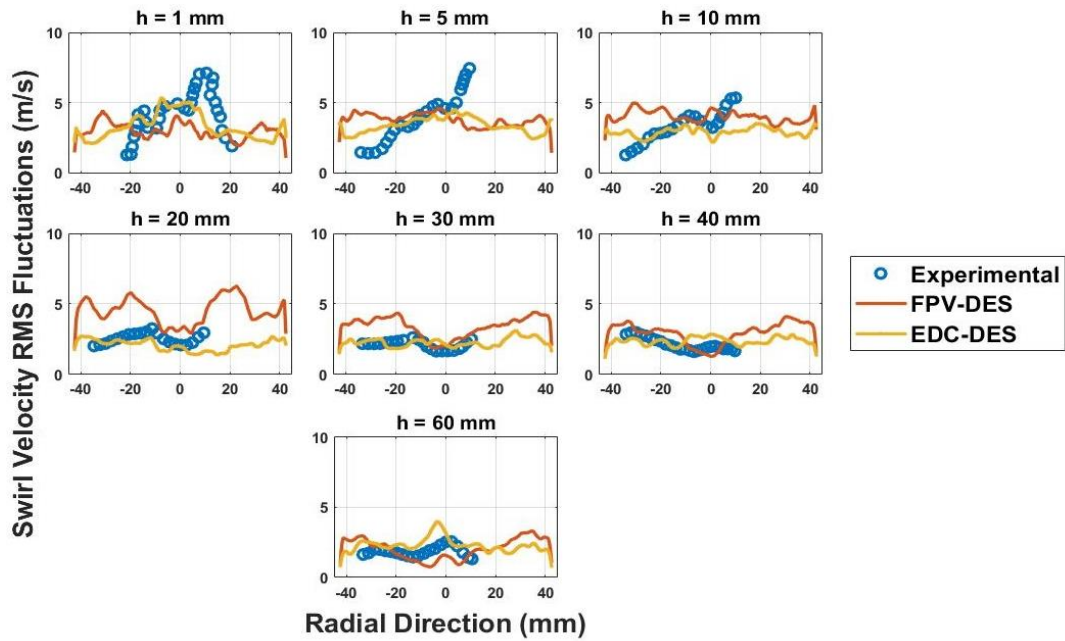
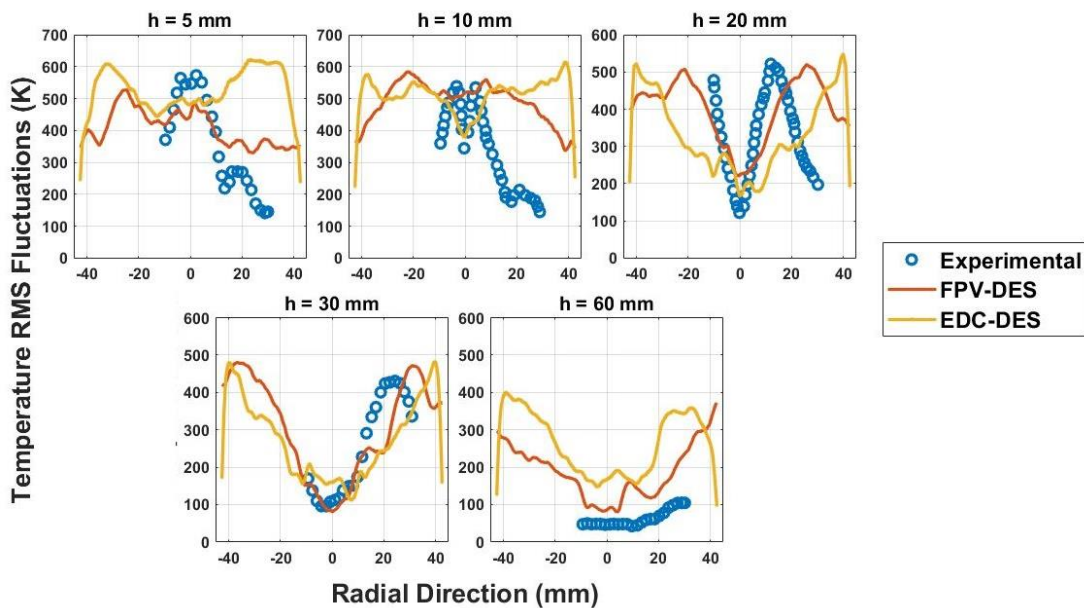Figure 5.11: Swirl velocity RMS fluctuations for FPV and EDC models

Figure 5.12: Temperature RMS fluctuations for FPV and EDC models

The mean and instantaneous axial velocity contours predicted by the EDC model can be seen in **Figure 5.14**. The significantly wider profile of the IRZ can also be noticed in the instantaneous contours, where the recirculation is much more pronounced than its FPV counterpart in **Figure 5.13**. Even in the instantaneous axial velocity contours, the axial flow

can be seen dominating close to the wall, while the recirculation is quite dominant near the bottom of the chamber and away from the wall.

From the FPV and EDC temperature contours, shown in **Figure 5.15** and

Figure 5.16, it can be seen that FPV predicts high temperatures close to the equilibrium temperature further downstream as compared to EDC, which shows equilibrium temperature being reached quite close to the inlet nozzle. These observations are consistent with the temperature and species fraction profiles of both models, in which it was seen that the EDC case predicted significantly higher reaction rates at the near-inlet heights, which were facilitated by the quick mixing resulting from a flatter IRZ profile as opposed to the IRZ profile predicted by the FPV model.

The instantaneous and mean mixture fraction contours of the FPV case with the lean flammability limit ($f = 0.0465$) isolines are shown in **Figure 5.17**. The mean flammability limit isolines encapsulate regions where the mixture fraction is high enough for localized reactions to occur, and regions beyond that limit show consumption of methane. From the instantaneous contours, multiple such regions can be observed downstream of the nozzle, which shows localized reactions taking place instead of one continuous reaction zone. This observation is in line with the instantaneous temperature contours seen in **Figure 5.15** which show multiple zones of high temperature instead of a uniform temperature distribution. The mean mixture fraction contours show a uniform reduction of mixture fraction with lean flammability isolines quite close to the inlet, which shows a uniform consumption of fuel and is consolidated by the mean temperature contours.
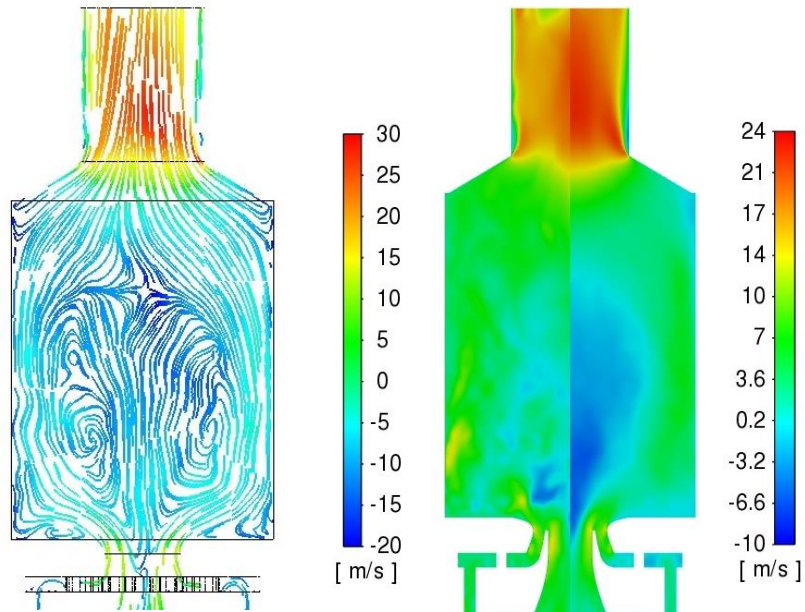
Figure 5.13: Mean velocity streamlines for the FPV model (left image), instantaneous (left-half) and mean axial velocity (right-half) contours for FPV (right image)
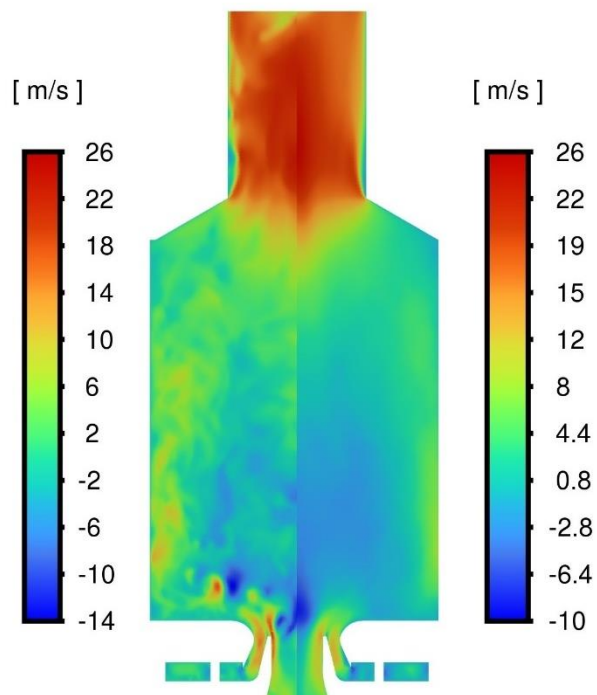

Figure 5.14: Instantaneous (left half) and mean axial velocity (right half) contours for EDC
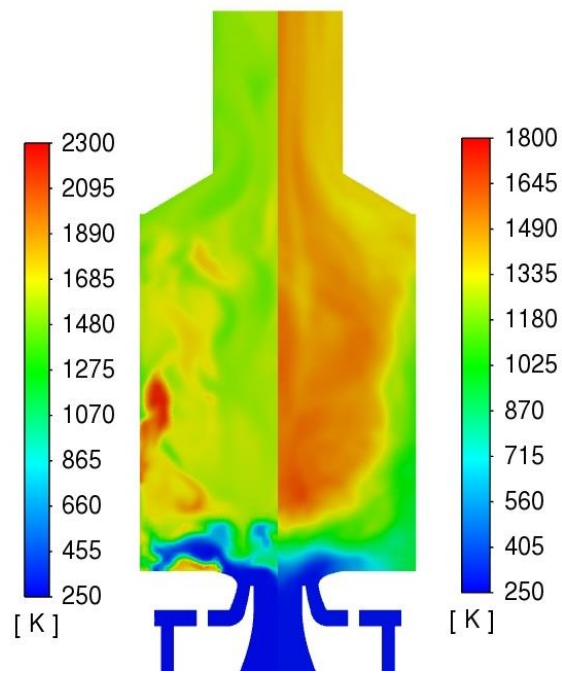
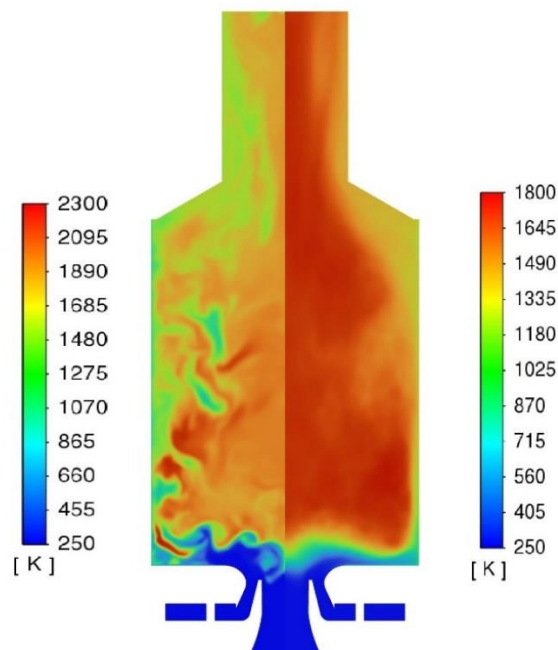**Figure 5.15:** instantaneous (left half) and mean (right half) temperature contours for FPV

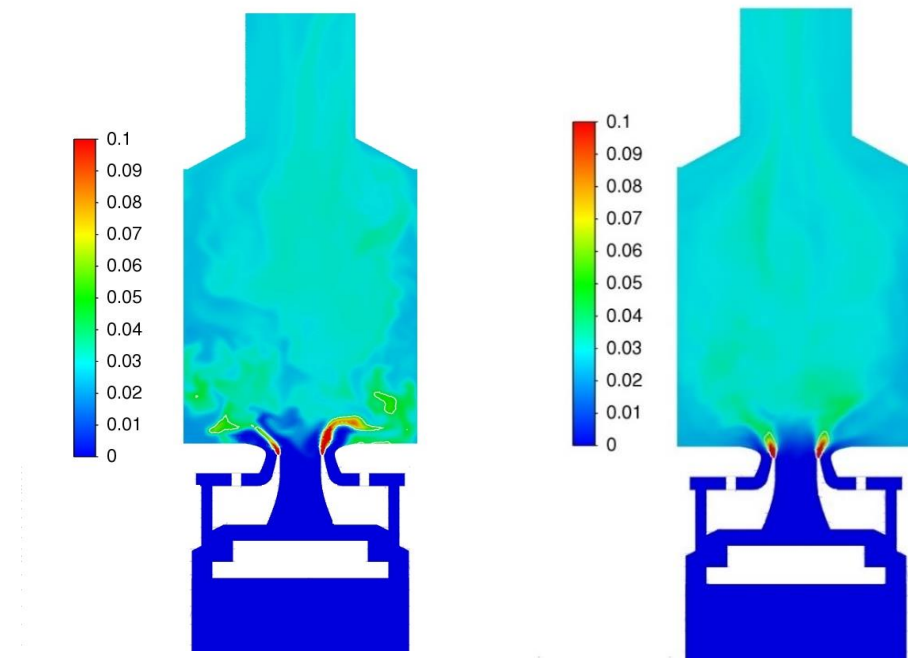**Figure 5.16:** instantaneous (left half) and mean (right half) temperature contours for EDC

Figure 5.17: instantaneous (left) and mean (right) mixture fraction contours for the FPV model with lean flammability limit isolines (f = 0.0465)

5.2 Parametric analysis results

Following the validation analysis and comparison between the FPV and EDC models, FPV was chosen to capture the turbulence-chemistry interactions for the parametric analysis, which compared the flow and thermochemical variations resulting from varying the inner swirler angle. The three configurations analyzed had inner swirler angles of 60 degrees, 62 degrees, and 64 degrees. The validation analysis was also performed on the 60 degrees configuration, due to which it was treated as the control case for this study.

The mean IRZ profiles for all 3 cases are shown in **Figure 5.18**
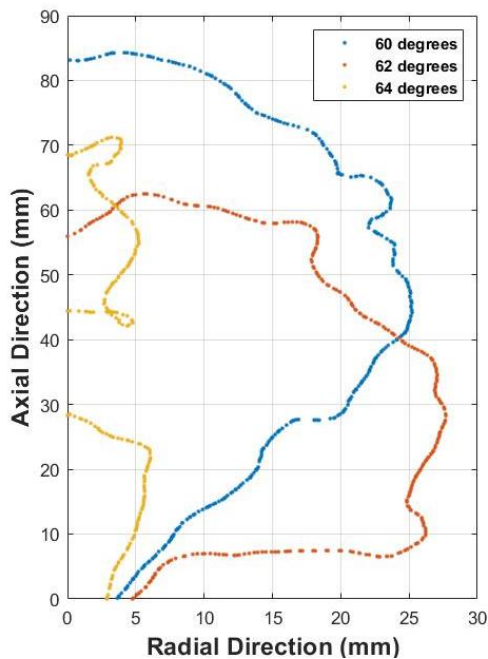
. There is a sharp contrast among all three profiles, with the IRZ of the 62 degrees configuration being flatter and broader compared to the 64 degrees case. The 64 degrees IRZ, however, has a rather unconventional shape, which shows 2 separate recirculation zones formed at the center, with the one penetrating the central nozzle having a much shorter and narrower profile compared to the other two. This shift in the IRZ profiles could be attributed to the change in the opening angle of the flow with increasing swirler angle. The opening angle of the flames is directly influenced by the interaction between the swirling air from the central and annular nozzles entering the chamber, and a drastically shorter IRZ profile indicates the flows from the 2 swirlers cancelling each other out upon entering the chamber.

The axial velocity profiles, shown in **Figure 5.19** depict the 64 degrees configuration having higher peak velocities than the other two configurations while having the shortest IRZ depth, which is in line with the IRZ profiles. The 62 degrees profile has the shortest peaks which is consistent with the significantly higher width of its IRZ compared to the other 2 cases. In the downstream regions, the 60 degrees configuration shows gradual reduction of its troughs, while the other 2 cases show relatively flatter profiles at h = 60mm.
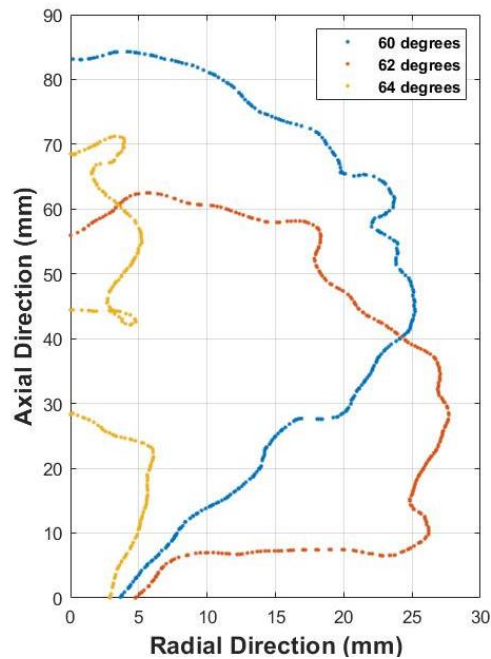
Figure 5.18: Mean u=0 isolines (IRZ shear layer) comparison between three dual swirl combustor configurations with increasing swirler angles

The radial velocity profiles, depicted in **Figure 5.20** show the 64 degrees configuration achieving much less radial velocities compared to the other 2 cases. The 62 degrees configuration has considerably higher radial velocities for the near inlet heights of h = 1mm and h = 5mm compared to the other 2 cases, which is followed by a sudden flattening of the profiles for downstream regions. This behaviour indicates that the radial distribution of the species is the highest for near-inlet heights and considerably lower for downstream heights. In comparison, the 60 degrees profiles show a gradual flattening for downstream heights, which implies better radial distribution of species in downstream regions. The flow behaviour indicated by the axial and radial velocity profiles is consolidated by the swirl velocity profiles in **Figure 5.21**, which show the 64 degrees profiles flattening past the height of 30mm. The swirl velocity profiles also imply that the 62 degrees configuration experiences the highest swirl strength among the 3 cases based on relatively higher velocity values in the downstream regions compared to the other 2 cases.

The instantaneous and mean axial velocity contours outlined by the isolines of zero axial velocity for the 64 degrees configuration are shown in **Figure 5.22**. Besides the narrow IRZ profile in the mean velocity contours, another interesting feature resulting from this configuration is the highly dominant outer recirculation zone (ORZ) extending from the bottom of the chamber to a greater height than that of the IRZ. It is to be noted that the 60 degrees

74

configuration, which was covered extensively in the previous section, featured a considerably weaker ORZ. The highly pronounced ORZ in the 64 degrees configuration can be explained by the narrow opening angle of the flow, which causes a greater degree of flow separation along the curvature of the annular nozzle. The part of the flow separating from the annular nozzle spreads radially and originates the outer recirculation zone, which is evident in the axial velocity contours. This behaviour implies a greater degree of mixing of species in the ORZ compared to the IRZ.

The time-averaged temperature profiles are shown in Figure 5.23. At h = 5mm, the 62 degrees profile shows relatively higher temperature values, which can be explained by the highly pronounced IRZ at that height compared to the other 2 cases and a higher radial distribution of species resulting from high radial velocities in the near-inlet region. The near-centreline temperature values of the 64 degrees profile are a result of its shrunk IRZ which results in much lower level of mixing compared to the other 2 cases. However, the near wall temperatures of the 64 degrees case are considerably higher at near-inlet heights compared to the other 2 cases, which can be explained by the dominant outer recirculation zone causing quick mixing of species in the near-wall region. All 3 cases attain near-equilibrium temperatures by the height of 40mm, with the 64 degrees profiles indicating that much of the reactions take place in the near wall region as opposed to the IRZ dominated reactions in the other 2 cases.
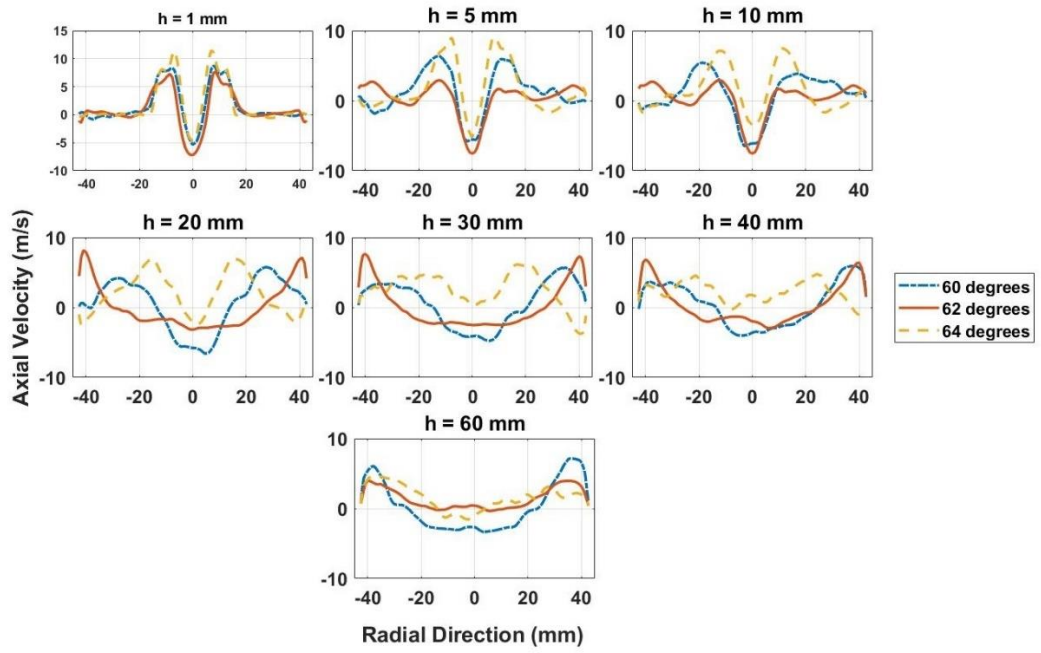
Figure 5.19: Mean Axial Velocity comparison between three dual swirl combustor configurations with increasing swirler angles
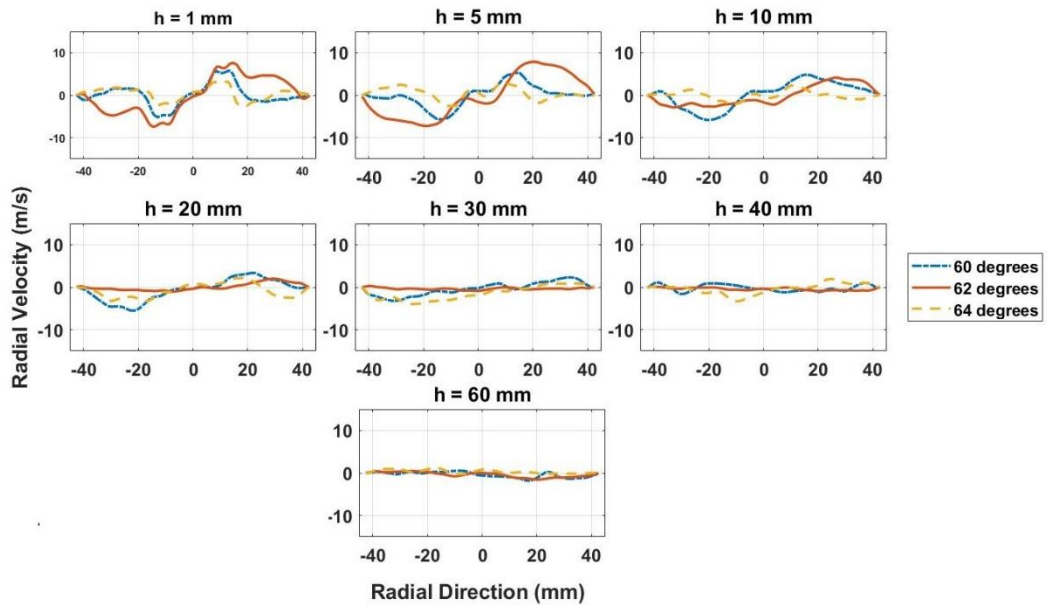

Figure 5.20: Mean radial velocity comparison between three dual swirl combustor configurations with increasing swirler angles
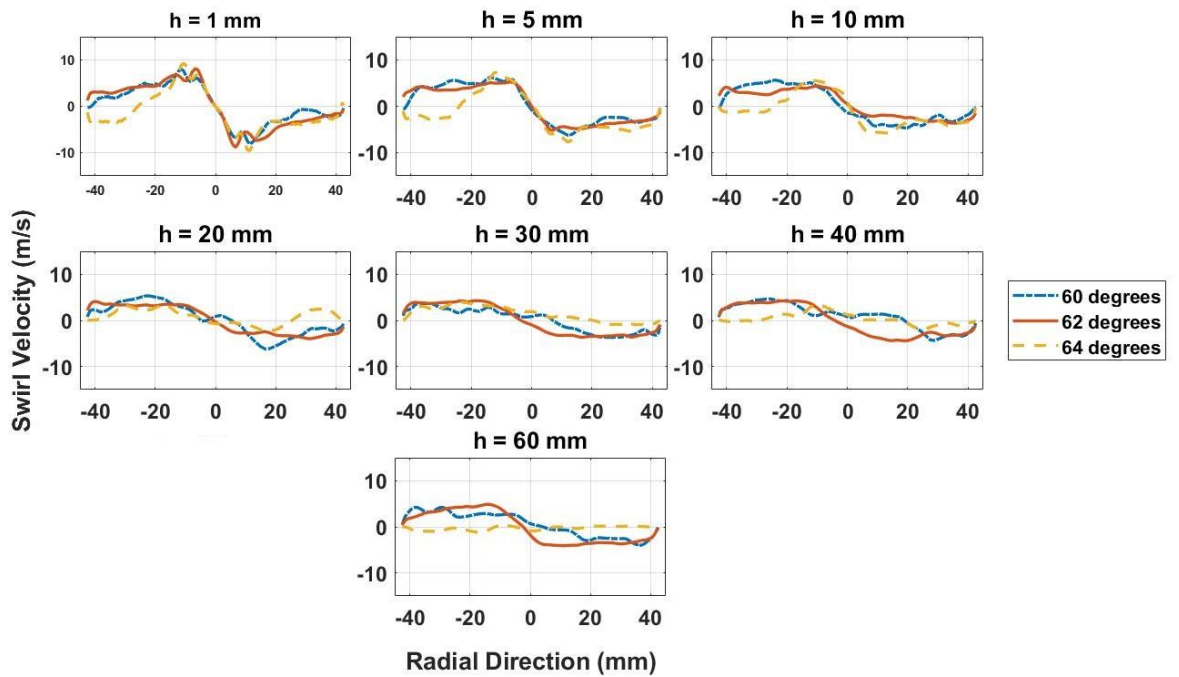
76

Figure 5.21: Mean swirl velocity comparison between three dual swirl combustor configurations with increasing swirler angles
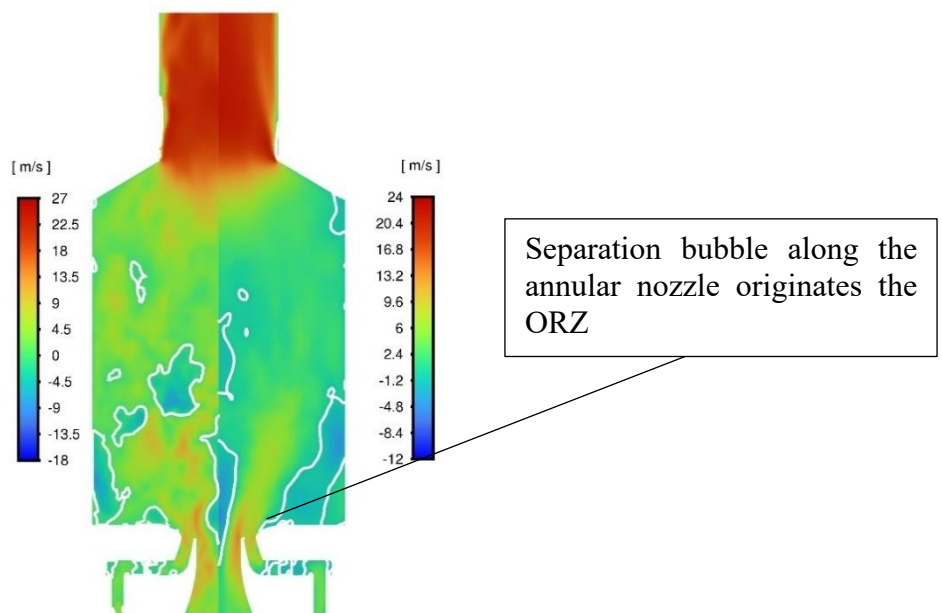

Figure 5.22: Axial Velocity contours of instantaneous (left half) and mean (right half) values for the 64 degrees configurations with u = 0 isolines

The mixture fraction profiles, shown in **Figure 5.24**, consolidate the assumptions made from the temperature profiles, as it can be seen that the peak mixture fraction values at lower heights are significantly higher for the 64 degrees case as compared to the other 2 cases. The mixture fraction profile of the 64 degrees case becomes uniform around the same value as the near wall values at the height of 5mm, which indicates that reactions are instigated mostly by the ORZ mixing. The time-averaged temperature contours of the 64 degrees case, shown in **Figure 5.25** support this conclusion, as equilibrium temperature is achieved quite close to the chamber bottom in the near wall region. The mean mixture fraction contours of the 64 degrees case, shown in **Figure 5.26** depict a relatively vertical distribution of flow as compared to the 60 degrees case (**Figure 5.17**). It can also be seen that the distribution of high mass fraction zones (encapsulated by lean flammability limit isolines) is relatively vertical compared to that of the 60 degrees case, which implies that reactions mostly take place away from the centreline.
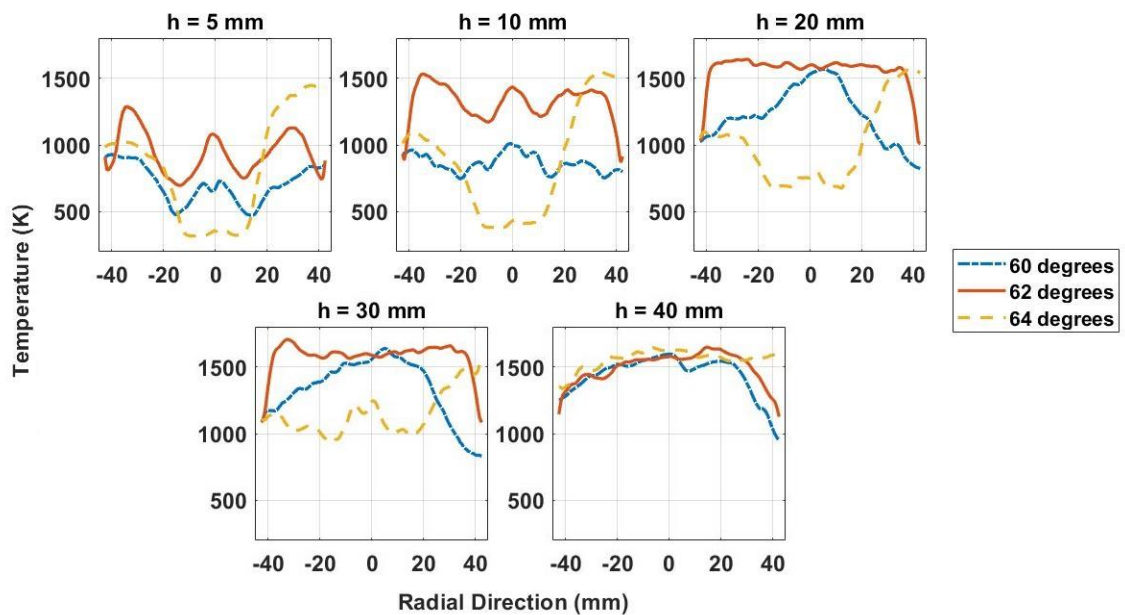

Figure 5.23: Mean temperature comparison between three dual swirl combustor configurations with increasing swirler angles
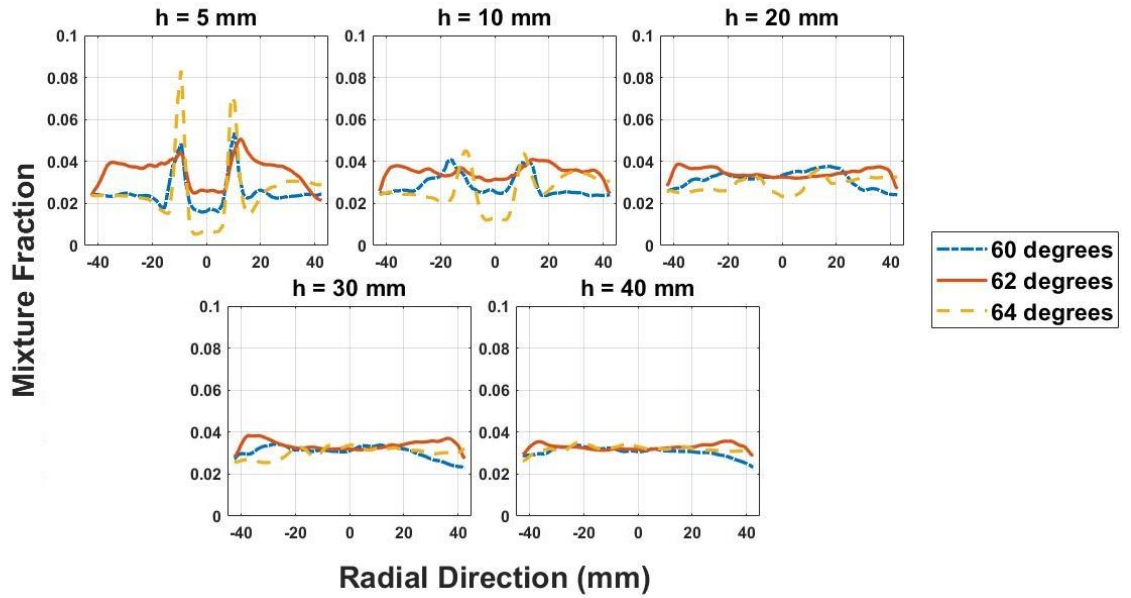
Figure 5.24: Mean mixture fraction comparison between three dual swirl combustor configurations with increasing swirler angles
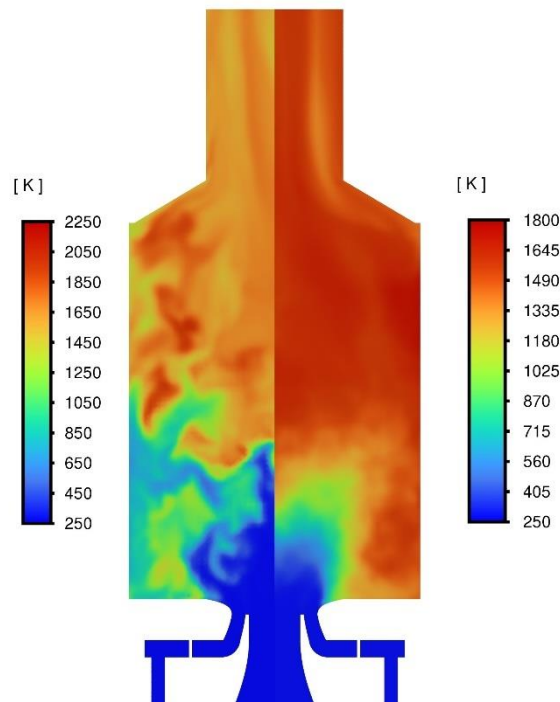

Figure 5.25: Temperature contours of instantaneous (left half) and mean (right half) values for the 64 degrees configurations with u = 0 isolines
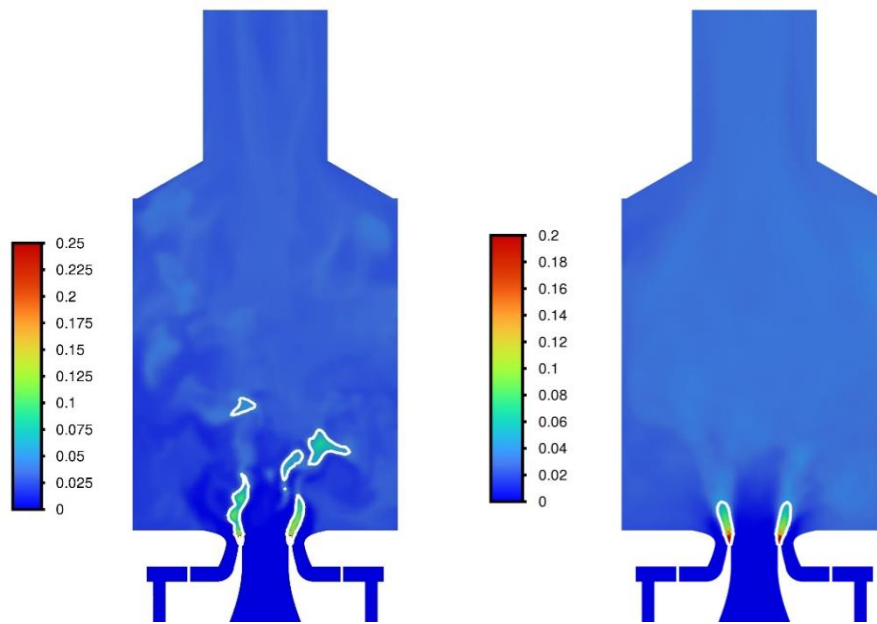
Figure 5.26 instantaneous (left) and mean (right) mixture fraction contours for the 64 degrees configuration with lean flammability limit (f = 0.0465) isolines

Chapter 6: CONCLUSION

This study performs numerical simulations of lean, dual swirl, partially premixed combustion using Detached Eddy Simulations (DES) as the turbulence model coupled with 2 different combustion models, namely Flamelet/Progress Variable approach (FPV) and Eddy Dissipation Concept (EDC) to validate a benchmark experimental study by DLR. It was observed that the FPV model replicated the flow dynamics and reaction kinetics with a greater accuracy compared to the EDC model, which predicted an underdeveloped inner recirculation zone and significantly high reaction rate. Certain discrepancies were observed in the FPV results like a considerably weak outer recirculation zone, which was a major deviation from experimental results.

The second phase of this study compared the flow behaviour and reaction kinetics of three distinct computational domains characterized by the unique inner swirler angles of 60, 62, and 64 degrees respectively. It was observed that the 62 degrees configuration resulted in flattened and wider inner recirculation zone compared to the 60 degrees configuration, while the 64 degrees configuration predicted much a narrower inner recirculation zone and jet opening, a possible reason for which could be the suppression of radial motion of the flow due to the interaction between the flows entering the chamber from the two upstream swirlers. The 64 degrees configuration also depicted an abnormally large outer recirculation zone which facilitated most of the mixing in the domain, leading to high reaction rates near the chamber walls.

6.1 Future Recommendations

Based on the predictions of the modelling techniques applied in this study and their subsequent results, the following recommendations are made for future work:

- Simulation of lean partially premixed flames close to blowoff using the LES turbulence model, the results of which can be compared to DES to determine the differences in their respective predictions.
- Performing numerical analysis using the same boundary conditions but applying adaptive meshing over a coarser mesh than the one used in this study to reduce the computational time.

- Parametrization of the annular nozzle curvature to observe the changes in flow behaviour resulting from different levels of curvature, since the curvature of the nozzle is crucial for accurate prediction of flow features like the axial velocity and the outer recirculation zone development.

- Numerical analysis of lean partially premixed flames focused on the influence of the pressure fluctuations on flow dynamics and reaction kinetics.

- Further parametrization of the swirler configurations to observe how various combinations of swirlers influence the thermochemical behaviour inside the chamber.

Bibliography

[1] D. S. Lee *et al.*, "The contribution of global aviation to anthropogenic climate forcing for 2000 to 2018," *Atmos Environ*, vol. 244, Jan. 2021, doi: 10.1016/j.atmosenv.2020.117834.

[2] R. C. Miake-Lye, A. Research, and D. Hauglustaine, "Impacts of Aviation NOx Emissions on Air Quality, Health, and Climate," 2022. [Online]. Available: https://www.icao.int/environmental-protection/Pages/environment-publications.aspx

[3] J. P. Appleton and J. B. Heywood, "The effects of imperfect fuel-air mixing in a burner onno formation from nitrogen in the air and the fuel," *Symposium (International) on Combustion*, vol. 14, no. 1, pp. 777–786, 1973, doi: https://doi.org/10.1016/S0082-0784(73)80072-4.

[4] J. E. Broadwell, W. J. A. Dahm, and M. G. Mungal, "Blowout of turbulent diffusion flames," *Symposium (International) on Combustion*, vol. 20, no. 1, pp. 303–310, 1984, doi: https://doi.org/10.1016/S0082-0784(85)80515-4.

[5] D. Han and M. G. Mungal, "Observations on the transition from flame liftoff to flame blowout," *Proceedings of the Combustion Institute*, vol. 28, no. 1, pp. 537–543, 2000, doi: https://doi.org/10.1016/S0082-0784(00)80253-2.

[6] F. E. C. Culick and V. Yang, "Prediction of the Stability of Unsteady Motions in Solid-Propellant Rocket Motors," *Nonsteady Burning and Combustion Stability of Solid Propellants*, vol. 143, pp. 719–779, 1992, doi: https://doi.org/10.2514/5.9781600866159.0719.0779.

[7] H.-J. Bauer, "New low emission strategies and combustor designs for civil aeroengine applications," *Progress in Computational Fluid Dynamics*, vol. 4, no. 5, pp. 130–142, 2004, doi: https://doi.org/10.1504/PCFD.2004.004081.

[8] P. Weigand, W. Meier, X. R. Duan, W. Stricker, and M. Aigner, "Investigations of swirl flames in a gas turbine model combustor: I. Flow field, structures, temperature, and species distributions," *Combust Flame*, vol. 144, no. 1–2, pp. 205–224, Jan. 2006, doi: 10.1016/j.combustflame.2005.07.010.

[9] W. Meier, X. R. Duan, and P. Weigand, "Investigations of swirl flames in a gas turbine model combustor: II. Turbulence-chemistry interactions," *Combust Flame*, vol. 144, no. 1–2, pp. 225–236, Jan. 2006, doi: 10.1016/j.combustflame.2005.07.009.

[10] T. Poinsot and D. Veynante, *Theoretical and Numerical Combustion*, 2nd ed. R.T. Edwards, 2005.

[11] D. G. Nicol, P. C. Malte, A. J. Hamer, R. J. Roby, and R. C. Steele, "Development of a Five-Step Global Methane Oxidation-NO Formation Mechanism for Lean-Premixed Gas Turbine Combustion," *J Eng Gas Turbine Power*, vol. 121, no. 2, pp. 272–280, 1999, doi: https://doi.org/10.1115/1.2817117.

[12]   D. Anderson, "Effects of equivalence ratio and dwell time on exhaust emissions from an experimental premixing prevaporizing burner," *American Society of Mechanical Engineers*, vol. 79771, 1975, doi: https://doi.org/10.1115/75-GT-69.

[13]   F. A. Williams, *Combustion Theory*, 2nd ed. Westview Press, 1994.

[14]   H. K. Versteeg and W. Malalasekera, *An Introduction to Computational Fluid Dynamics Second Edition*, 2nd ed. Pearson Education Limited, 2007. [Online]. Available: www.pearsoned.co.uk/versteeg

[15]   P. A. Durbin, "A perspective on recent developments in rans modeling," *Engineering Turbulence Modelling and Experiments*, 2002, doi: https://doi.org/10.1016/B978-008044114-6/50002-8.

[16]   Y. Zhiyin, "Large-eddy simulation: Past, present and the future," *Chinese Journal of Aeronautics*, vol. 28, no. 1, pp. 11–24, Feb. 2015, doi: 10.1016/j.cja.2014.12.007.

[17]   J. Smagorinsky, "General circulation experiments with the primitive equations," *Mon Weather Rev*, vol. 91, no. 3, pp. 99–164, 1963, doi: https://doi.org/10.1175/1520-0493(1963)091%3C0099:GCEWTP%3E2.3.CO;2.

[18]   T. Kajishima and T. Nomachi, "One-equation subgrid scale model using dynamic procedure for the energy production," *Journal of Applied Mechanics, Transactions ASME*, vol. 73, no. 3, pp. 368–373, May 2006, doi: 10.1115/1.2164509.

[19]   M. Germano, U. Piomelli, P. Moin, and W. H. Cabot, "A dynamic subgrid-scale eddy viscosity model," *Physics of Fluids A*, vol. 3, no. 7, pp. 1760–1765, 1991, doi: 10.1063/1.857955.

[20]   P. R. Spalart, "Detached-eddy simulation," *Annu Rev Fluid Mech*, vol. 41, pp. 181–202, Jan. 2009, doi: 10.1146/annurev.fluid.010908.165130.

[21]   U. Bunge, C. Mockett, and F. Thiele, "Guidelines for implementing Detached-Eddy Simulation using different models," *Aerosp Sci Technol*, vol. 11, no. 5, pp. 376–385, Jun. 2007, doi: 10.1016/j.ast.2007.02.001.

[22]   "Detached Eddy Simulations (From ANSYS User Guide 12.0)." Accessed: Sep. 12, 2024. [Online]. Available: https://www.afs.enea.it/project/neptunius/docs/fluent/html/th/node88.htm

[23]   A. Ben Sik Ali, W. Kriaa, H. Mhiri, and P. Bournot, "Detached-Eddy Simulations (DES) of a complex swirl stabilized gas turbine model combustor," *International Journal of Energy and Environment*, vol. 7, no. 5, pp. 2076–2909, 2016, doi: https://api.semanticscholar.org/CorpusID:231968309.

[24]   H. C. Hottel and W. R. Hawthorne, "Diffusion in laminar flame jets," *Symposium on Combustion and Flame, and Explosion Phenomena*, vol. 3, no. 1, pp. 254–266, 1948, doi: https://doi.org/10.1016/S1062-2896(49)80034-1.

[25]   R. W. Bilger, "Turbulent diffusion flames," *Annu Rev Fluid Mech*, vol. 21, no. 1, pp. 101–136, 1989, doi: https://doi.org/10.1146/annurev.fl.21.010189.000533.

[26]   N. Peters, "Laminar diffusion flamelet models in non-premixed turbulent combustion," *Prog Energy Combust Sci*, vol. 10, pp. 319–339, 1984, doi: https://doi.org/10.1016/0360-1285(84)90114-X.

[27]   J. Y. Chen, W. Kollmann, and R. W. Dibble, "PDF modeling of turbulent nonpremixed methane jet flames," *Combustion Science and Technology*, vol. 64, no. 4–6, pp. 315–346, Apr. 1989, doi: 10.1080/00102208908924038.

[28]   T. J. Poinsot and D. P. Veynante, "Combustion," in *Encyclopedia of Computational Mechanics*, vol. 3, 2004, pp. 499–523.

[29]   A. M. Steinberg, P. E. Hamlington, and X. Zhao, "Structure and dynamics of highly turbulent premixed combustion," *Prog Energy Combust Sci*, vol. 85, p. 100900, 2021, doi: 10.1016/j.pecs.2020.10.

[30]   S. B. Pope, "Turbulent premixed flames," *Ann. Rev. Fluid Mech*, vol. 19, pp. 237–70, 1987, doi: https://doi.org/10.1146/annurev.fl.19.010187.001321.

[31]   K. N. C. Bray and J. B. Moss, "A unified statistical model of the premixed turbulent flame," *Acta Astronaut*, vol. 4, pp. 291–319, 1977, doi: https://doi.org/10.1016/0094-5765(77)90053-4.

[32]   C. J. Rallis and A. M. Garforth, "The determination of laminar burning velocity," *Prog. Energy Combust. Sci*, vol. 6, pp. 303–329, 1980, doi: https://doi.org/10.1016/0360-1285(80)90008-8.

[33]   J. Gottgens, F. Mauss, and N. Peters, "Analytic approximations of burning velocities and flame thicknesses of lean hydrogen," in *Twenty-Fourth Symposium (International) on Combustion/The Combustion Institute*, 1992, pp. 129–135. doi: https://doi.org/10.1016/S0082-0784(06)80020-2.

[34]   J. Abraham, F. A. Williams, and F. V Bracco, "A Discussion of Turbulent Flame Structure in Premixed Charges," *SAE Transactions*, vol. 94, pp. 128–143, 1985, doi: https://www.jstor.org/stable/44467411.

[35]   K. N. C. Bray, "Turbulent Flows with Premixed Reactants," in *Turbulent Reacting Flows* , 1980, pp. 115–183. doi: doi.org/10.1007/3540101926_10.

[36]   N. Peters, "Laminar flamelet concepts in turbulent combustion," in *Fwenty-first Symposium (International) on Combustion/The Combustion Institute*, 1986, pp. 1231–1250. doi: https://doi.org/10.1016/S0082-0784(88)80355-2.

[37]   P. Clavin, "Premixed combustion and gasdynamics," *Annu. Rev. Fluid Mech*, vol. 26, pp. 321–52, 1994, doi: https://doi.org/10.1146/annurev.fl.26.010194.001541.

[38]   V. L. Zimont, "Gas premixed combustion at high turbulence. Turbulent flame closure combustion model," *Exp Therm Fluid Sci*, pp. 179–186, 2000, doi: https://ui.adsabs.harvard.edu/link_gateway/2000ETFS...21..179Z/doi:10.1016/S0894-1777(99)00069-2.

[39]   J. C. Massey, Z. X. Chen, and N. Swaminathan, "Lean Flame Root Dynamics in a Gas Turbine Model Combustor," *Combustion Science and Technology*, vol. 191, no. 5–6, pp. 1019–1042, Jun. 2019, doi: 10.1080/00102202.2019.1584616.

[40]   N. Peters, *Turbulent Combustion*, 1st ed. Cambridge University Press, 2000.

[41]   S. Kimura, O. Aoki, H. Ogawa, S. Muranaka, and Y. Enomoto, "New Combustion Concept for Ultra-Clean and High-Efficiency Small DI Diesel Engines," *SAE Technical Paper 1999-01-3681*, 1999, doi: https://doi.org/10.4271/1999-01-3681.

[42]   K. Wohl, N. M. Kapp, and C. Gazley, "The Stability of Open Flames," *Symposium on Combustion and Flame, and Explosion Phenomena*, vol. 3, no. 1, pp. 3–21, 1948, doi: https://doi.org/10.1016/S1062-2896(49)80005-5.

[43]   N. Peters and F. A. Williams, "Liftoff characteristics of turbulent jet diffusion flames," *AIAA Journal*, vol. 21, no. 3, pp. 423–429, 1983, doi: 10.2514/3.8089.

[44]   S. Donnerhack and N. Peters, "Stabilization heights in lifted Methane-Air jet diffusion flames diluted with nitrogen," *Combustion Science and Technology*, vol. 41, no. 1–2, pp. 101–108, 1984, doi: 10.1080/00102208408923825.

[45]   J. W. Dold, "Analysis of a Slowly Varying Triple Flame," *Combust Flame*, vol. 76, pp. 71–88, 1989, doi: https://doi.org/10.1016/0010-2180(89)90079-5.

[46]   G. Damkohler, "The effect of turbulence on the flame velocity in gas mixtures," *Zeitschrift fuer Elektrochemie und Angewandte Physikalische Chemiw* , vol. 46, no. 11, 1940, doi: https://ntrs.nasa.gov/citations/20050009802.

[47]   M. Herrmann, "Numerische simulation vorgemischter und teilweise vorgemischter turbulenten flamen," RWTH, Aachen, 2000.

[48]   M. Chen, M. Herrmann, and N. Peters, "Flamelet modeling of lifted turbulent methane/air and propane/air jet diffusion flames," *Proceedings of the Combustion Institute*, vol. 28, pp. 167–174, 2000, doi: https://doi.org/10.1016/S0082-0784(00)80208-8.

[49]   B. Magnussen, "On the structure of turbulence and a generalized eddy dissipation concept for chemical reaction in turbulent flow," in *19th Aerospace Science Meeting*, American Institute of Aeronautics and Astronautics, 1981. doi: https://doi.org/10.2514/6.1981-42.

[50]   B. F. Magnussen, "Modeling of NOx and Soot Formation by the Eddy Dissipation Concept," in *Int. Flame Res. Found*, 1989. doi: https://folk.ntnu.no/ivarse/edc/EDC1989.pdf.

[51]   M. J. Evans, P. R. Medwell, and Z. F. Tian, "Modeling Lifted Jet Flames in a Heated Coflow using an Optimized Eddy Dissipation Concept Model," *Combustion Science and Technology*, vol. 187, no. 7, pp. 1093–1109, Jul. 2015, doi: 10.1080/00102202.2014.1002836.

[52] M. Bösenhofer, E. M. Wartha, C. Jordan, and M. Harasek, "The eddy dissipation concept-analysis of different fine structure treatments for classical combustion," *Energies (Basel)*, vol. 11, no. 7, 2018, doi: 10.3390/en11071902.

[53] I. R. Gran and B. F. Magnussen, "A numerical study of a bluff-body stabilized diffusion flame. Part 2. Influence of combustion modeling and finite-rate chemistry," *Combustion Science and Technology*, vol. 119, no. 1–6, pp. 191–217, 1996, doi: 10.1080/00102209608951999.

[54] B. F. Magnussen, "The eddy dissipation concept-a bridge between science and technology," in *ECCOMAS Thematic Conference on Computational Combustion*, Lisbon, Jun. 2005. doi: https://api.semanticscholar.org/CorpusID:67818474.

[55] A. Parente, M. R. Malik, F. Contino, A. Cuoci, and B. B. Dally, "Extension of the Eddy Dissipation Concept for turbulence/chemistry interactions to MILD combustion," *Fuel*, vol. 163, pp. 98–111, Jan. 2016, doi: 10.1016/j.fuel.2015.09.020.

[56] N. Peters, "Local Quenching Due to Flame Stretch and Non-Premixed Turbulent Combustion," *Combustion Science and Technology*, vol. 30, no. 1–6, pp. 1–17, Jan. 1983, doi: 10.1080/00102208308923608.

[57] C. D. Pierce and P. Moin, "Progress-variable approach for large-eddy simulation of non-premixed turbulent combustion," *J Fluid Mech*, vol. 504, pp. 73–97, Apr. 2004, doi: 10.1017/S0022112004008213.

[58] M. Ihme, C. M. Cha, and H. Pitsch, "Prediction of local extinction and re-ignition effects in non-premixed turbulent combustion using a flamelet/progress variable approach," *Proceedings of the Combustion Institute*, vol. 30, no. 1, pp. 793–800, 2005, doi: 10.1016/j.proci.2004.08.260.

[59] J. Janicka and W. Kollmann, "A two-variables formalism for the treatment of chemical reactions in turbulent h2-air diffusion flames," in *Proceedings of the 17th Symposium (Intl.) On Combustion*, Leeds, 1978, pp. 421–430. doi: https://doi.org/10.1016/S0082-0784(79)80043-0.

[60] P. Bruel, B. Rogg, and K. N. C. Bray, "On auto-ignition in laminar and turbulent non-premixed systems," *Symposium (International) on Combustion*, vol. 23, no. 1, pp. 759–766, 1990, doi: https://doi.org/10.1016/S0082-0784(06)80327-9.

[61] B. Magnussen and B. Hjertager, "On mathematical modeling of turbulent combustion with special emphasis on soot formation and combustion," in *Sixteenth Symposium on Combustion, The Combustion Institute*, 1976.

[62] P. Wang, "The model constant A of the eddy dissipation model," *Progress in Computational Fluid Dynamics*, vol. 16, no. 2, pp. 118–125, 2016, [Online]. Available: http://www.sandia.gov/TNF/

[63] J. A. van Oijen and L. P. H. de Goey, "Modelling of premixed laminar flames using flamelet-generated manifolds," *Combustion Science and Technology*, vol. 161, no. 1, pp. 113–137, 2000, doi: 10.1080/00102200008935814.

[64] H. A. El-Asrag and G. Golden, "A comparison between two different Flamelet reduced order manifolds for non-premixed turbulent flames," in *8th U. S. National Combustion Meeting*, The Combustion Institute, May 2013.

[65] S. Navarro-Martinez, A. Kronenburg, and F. Di Mare, "Conditional Moment Closure for Large Eddy Simulations," *Flow Turbul Combust*, vol. 75, pp. 245–274, 2005.

[66] A. Y. Klimenko and R. W. Bilger, "Conditional moment closure for turbulent combustion," *Prog Energy Combust Sci*, vol. 25, pp. 595–687, 1999, [Online]. Available: www.elsevier.com/locate/pecs

[67] O. Colin, F. Ducros, D. Veynante, and T. Poinsot, "A thickened flame model for large eddy simulations of turbulent premixed combustion," *Physics of Fluids*, vol. 12, no. 7, pp. 1843–1863, 2000, doi: 10.1063/1.870436.

[68] A. R. Kerstein, W. T. Ashurst, and F. A. W'illiams, "Field equation for interface propagation in an unsteady homogeneous flow Seld," *Phys Rev A Gen Phys*, vol. 37, no. 7, pp. 2728–2731, 1988.

[69] M. Boger, D. Veynante, H. Boughanem, and A. Trouvé, "Direct numerical simulation analysis of flame surface density concept for large eddy simulation of turbulent premixed combustion," *Symposium (International) on Combustion*, vol. 27, no. 1, pp. 917–925, 1998.

[70] C. K. Westbrook and F. L. Dryer, "Chemical kinetic modeling of hydrocarbon combustion," *Prog Energy Combust Sci*, vol. 10, no. 1, pp. 1–57, 1984.

[71] F. L. Dryer and I. Glassman, "High-temperature oxidation of CO and CH4," *Symposium (International) on Combustion*, vol. 14, no. 1, pp. 987–1003, 1973.

[72] V. Dupont, M. Pourkashanian, and A. Williams, "Modeling of Process Heaters Fired by Natural Gas," *Journal of The Institute of Energy*, vol. 66, pp. 20–28, 1993.

[73] W. P. Jones and R. P. Lindstedt, "Global Reaction Schemes for Hydrocarbon Combustion," *Combust Flame*, vol. 73, no. 3, pp. 233–249, 1988, doi: https://doi.org/10.1016/0010-2180(88)90021-1.

[74] D. G. Nicol, "A Chemical and Numerical Study of NOx and Pollutant Formation in Low-Emissions Combustion," PhD Dissertation, University of Washington, , Saint Louis, 1995. [Online]. Available: https://www.proquest.com/openview/615bf384b581a12cb1ccd6fd0380b54b/1?cbl=187 50&diss=y&pq-origsite=gscholar&parentSessionId=eFj6Nz6Eq%2B3ZwkcN0Eyk%2Ftvzpa6vOlescr 2tsBzLL2k%3D

[75] G. P. Smith *et al.*, "GRI-Mech 3.0." [Online]. Available: http://www.me.berkeley.edu/gri_mech/

[76] A. Kazakov and M. Frenklach, "Reduced reaction sets based on GRI-Mech 1.2." [Online]. Available: http://www.me.berkeley.edu/drm/

[77] C. J. Sung, C. K. Law, and J.-Y. Chen, "An augmented reduced mechanism for methane oxidation with comprehensive global parametric validation," *Symposium (International) on Combustion*, vol. 27, no. 1, pp. 295–304, 1998.

[78] A. Bahramian, "CFD Insight of the Flow Dynamics and Velocity Fields in a Gas Turbine Combustor with a Swirl Flame," *Iranian Journal of Chemical Engineering*, vol. 12, no. 2, 2015.

[79] A. Bahramian, M. Maleki, and B. Medi, "CFD modeling of flame structures in a gas turbine combustion reactor: Velocity, temperature, and species distribution," *International Journal of Chemical Reactor Engineering*, vol. 15, no. 4, Aug. 2017, doi: 10.1515/ijcre-2016-0076.

[80] A. Mardani and A. Fazlollahi-Ghomshi, "Numerical Investigation of a Double-Swirled Gas Turbine Model Combustor Using a RANS Approach with Different Turbulence-Chemistry Interaction Models," *Energy and Fuels*, vol. 30, no. 8, pp. 6764–6776, Aug. 2016, doi: 10.1021/acs.energyfuels.6b00452.

[81] A. Mardani, B. Asadi, and A. A. Beige, "Investigation of flame structure and precessing vortex core instability of a gas turbine model combustor with different swirler configurations," *Physics of Fluids*, vol. 34, no. 8, Aug. 2022, doi: 10.1063/5.0097430.

[82] A. C. Benim, S. Iqbal, W. Meier, F. Joos, and A. Wiedermann, "Numerical investigation of turbulent swirling flames with validation in a gas turbine model combustor," *Appl Therm Eng*, vol. 110, pp. 202–212, Jan. 2017, doi: 10.1016/j.applthermaleng.2016.08.143.

[83] Y. C. See and M. Ihme, "Large eddy simulation of a partially-premixed gas turbine model combustor," in *Proceedings of the Combustion Institute*, Elsevier Ltd, 2015, pp. 1225–1234. doi: 10.1016/j.proci.2014.08.006.

[84] M. Ihme and H. Pitsch, "Prediction of extinction and reignition in nonpremixed turbulent flames using a flamelet/progress variable model. 1. A priori study and presumed PDF closure," *Combust Flame*, vol. 155, no. 1–2, pp. 70–89, Oct. 2008, doi: 10.1016/j.combustflame.2008.04.001.

[85] B. Fiorina, R. Vicquelin, P. Auzillon, N. Darabiha, O. Gicquel, and D. Veynante, "A filtered tabulated chemistry model for LES of premixed combustion," *Combust Flame*, vol. 157, no. 3, pp. 465–475, Mar. 2010, doi: 10.1016/j.combustflame.2009.09.015.

[86] P. Auzillon, O. Gicquel, N. Darabiha, D. Veynante, and B. Fiorina, "A Filtered Tabulated Chemistry model for LES of stratified flames," *Combust Flame*, vol. 159, no. 8, pp. 2704–2717, Aug. 2012, doi: 10.1016/j.combustflame.2012.03.006.

[87] D. Huang, J. Xu, R. Chen, and H. Meng, "Large eddy simulations of turbulent combustion of kerosene-air in a dual swirl gas turbine model combustor at high pressures," *Fuel*, vol. 282, Dec. 2020, doi: 10.1016/j.fuel.2020.118820.

[88] Z. X. Chen, N. Swaminathan, M. Stöhr, and W. Meier, "Interaction between self-excited oscillations and fuel-air mixing in a dual swirl combustor," *Proceedings of the Combustion Institute*, vol. 37, no. 2, pp. 2325–2333, 2019, doi: 10.1016/j.proci.2018.08.042.

[89] Z. X. Chen and N. Swaminathan, "Influence of fuel plenum on thermoacoustic oscillations inside a swirl combustor," *Fuel*, vol. 275, Sep. 2020, doi: 10.1016/j.fuel.2020.117868.

[90] Z. X. Chen, I. Langella, N. Swaminathan, M. Stöhr, W. Meier, and H. Kolla, "Large Eddy Simulation of a dual swirl gas turbine combustor: Flame/flow structures and stabilisation under thermoacoustically stable and unstable conditions," *Combust Flame*, vol. 203, pp. 279–300, May 2019, doi: 10.1016/j.combustflame.2019.02.013.

[91] J. C. Massey, Z. X. Chen, and N. Swaminathan, "Modelling Heat Loss Effects in the Large Eddy Simulation of a Lean Swirl-Stabilised Flame," *Flow Turbul Combust*, vol. 106, no. 4, pp. 1355–1378, Apr. 2021, doi: 10.1007/s10494-020-00192-4.

[92] F. Proch and A. M. Kempf, "Modeling heat loss effects in the large eddy simulation of a model gas turbine combustor with premixed flamelet generated manifolds," *Proceedings of the Combustion Institute*, vol. 35, no. 3, pp. 3337–3345, 2015, doi: 10.1016/j.proci.2014.07.036.

[93] N. Arnold-Medabalimi, C. Huang, and K. Duraisamy, "Large-eddy simulation and challenges for projection-based reduced-order modeling of a gas turbine model combustor," *International Journal of Spray and Combustion Dynamics*, vol. 14, no. 1–2, pp. 153–175, Mar. 2022, doi: 10.1177/17568277221100650.

[94] J. C. Massey, Z. X. Chen, M. Stöhr, W. Meier, and N. Swaminathan, "On the blow-off correlation for swirl-stabilised flames with a precessing vortex core," *Combust Flame*, vol. 239, May 2022, doi: 10.1016/j.combustflame.2021.111741.

[95] A. Widenhorn, B. Noll, and M. Aigner, "Numerical characterisation of a gas turbine model combustor applying scale-adaptive simulation," in *ASME Turbo Expo 2009: Power for Land, Sea and Air*, Orlando, FL, 2009. doi: https://doi.org/10.1115/GT2009-59038.

[96] F. Rebosio, A. Widenhorn, B. Noll, and M. Aigner, "Numerical simulation of a gas turbine model combustor operated near the lean extinction limit," in *Proceedings of ASME Turbo Expo 2010: Power for Land, Sea and Air*, Glasgow: ASME, 2010, pp. 603–612. doi: http://dx.doi.org/10.1115/GT2010-22751.

[97] M. J. Wankhede, F. A. Tap, P. Schapotschnikow, and W. J. S. Ramaekers, "Numerical study of unsteady flow-field and flame dynamics in a gas turbine model combustor," in *Turbine Technical Conference and Exposition*, Düsseldorf: ASME, Jun. 2014. doi: https://doi.org/10.1115/GT2014-25784.

[98] A. Donini, R. J. Bastiaans, J. A. van Oijen, and L. H. Philip de Goey, "The implementation of five-dimensional fgm combustion model for the simulation of a gas turbine model combustor," in *Turbine Technical Conference and Exposition*, Montreal: ASME, Jun. 2015. doi: http://dx.doi.org/10.1115/GT2015-42037.

[99] A. Donini, R. J. M. Bastiaans, J. A. van Oijen, and L. P. H. de Goey, "A 5-D Implementation of FGM for the Large Eddy Simulation of a Stratified Swirled Flame with Heat Loss in a Gas Turbine Combustor," *Flow Turbul Combust*, vol. 98, no. 3, pp. 887–922, Apr. 2017, doi: 10.1007/s10494-016-9777-7.

[100] H. Zhang and E. Mastorakos, "LES/CMC Modelling of a Gas Turbine Model Combustor with Quick Fuel Mixing," *Flow Turbul Combust*, vol. 102, no. 4, pp. 909–930, Apr. 2019, doi: 10.1007/s10494-018-9988-1.

[101] P. Zhang, J. W. Park, B. Wu, and X. Zhao, "Large eddy simulation/thickened flame model simulations of a lean partially premixed gas turbine model combustor," *Combustion Theory and Modelling*, vol. 25, no. 7, pp. 1296–1323, 2021, doi: 10.1080/13647830.2021.1976421.

[102] T. F. Lu, C. S. Yoo, J. H. Chen, and C. K. Law, "Three-dimensional direct numerical simulation of a turbulent lifted hydrogen jet flame in heated coflow: A chemical explosive mode analysis," *J Fluid Mech*, vol. 652, pp. 45–64, 2010, doi: 10.1017/S002211201000039X.

[103] A. F. Sudarma and M. H. Morsy, "Numerical study of non-premixed air-methane swirl combustor flows using RANS method," in *IOP Conference Series: Materials Science and Engineering*, Institute of Physics Publishing, Nov. 2018. doi: 10.1088/1757-899X/453/1/012058.

[104] F. Rebosio, A. Widenhorn, B. Noll, and M. Aigner, "Numerical simulation of a gas turbine model combustor operated near the lean extinction limit," in *Proceedings of ASME Turbo Expo 2010: Power for Land, Sea and Air*, Glasgow: ASME, Jun. 2010, pp. 603–612. doi: http://dx.doi.org/10.1115/GT2010-22751

[105] C. K. Westbrook and F. L. Dryer, "Simplified Reaction Mechanisms for the Oxidation of Hydrocarbon Fuels in Flames," *Combustion Science and Technology*, vol. 27, no. 1–2, pp. 31–43, Dec. 1981, doi: 10.1080/00102208108946970.

[106] C. T. Bowman *et al.*, "GRI-Mech 2.11." Accessed: Dec. 03, 2023. [Online]. Available: http://combustion.berkeley.edu/gri-mech/

[107] M. Frenklach *et al.*, "GRI-Mech-an optimized detailed chemical reaction mechanism for methane combustion," Nov. 1995.

[108] S. B. Pope, "Computationally efficient implementation of combustion chemistry using in situ adaptive tabulation," *Combustion Theory and Modelling*, vol. 1, no. 1, pp. 41–63, 1997, doi: 10.1080/713665229.

[109] S. James, M. S. Anand, M. K. Razdan, and S. B. Pope, "In situ detailed chemistry calculations in combustor flow analyses," *J Eng Gas Turbine Power*, vol. 123, no. 4, pp. 747–756, Oct. 2001, doi: 10.1115/1.1384878.

[110] I. Reba, "Applications of the Coanda effect," *Sci Am*, vol. 214, no. 6, pp. 84–93, 1966.

[111] C. Lubert, "On Some Recent Applications of the Coanda Effect," *International Journal of Acoustics and Vibrations.*, vol. 16, no. 3, pp. 144–153, 2011, doi: https://doi.org/10.1121/1.3694201.

[112] W. J. S. Ramaekers, F. A. Tap, and B. J. Boersma, "Subgrid Model Influence in Large Eddy Simulations of Non-reacting Flow in a Gas Turbine Combustor," *Flow Turbul Combust*, vol. 100, no. 2, pp. 457–479, Mar. 2018, doi: 10.1007/s10494-017-9853-7.